AN ABSTRACT OF THE THESIS OF

Fei Teng for the degree of Master of Science in Materials Science presented on May 17, 2016.

Title: Role of Stoichiometry on Ordering in Ni-Cr Alloys

Abstract approved:

Julie D. Tucker

Mechanical property degradation due to isothermal ageing is of potential concern for alloys based on the Ni-Cr binary system (*e.g.*, Inconel 690, 625), particularly in nuclear power applications where component lifetimes can exceed 40 years. In the present research, the disorder-order phase transformation, which is the primary mechanism of ageing, has been studied in Ni-Cr model alloys with varying stoichiometry by a combined experimental and computational approach. Experimental measurements of the change in lattice parameter and micro-hardness as a function of aging time and temperature are obtained in order to assess the model accuracy. Samples with different stoichiometry undergo high accuracy isothermal ageing for up to 10,000 hours and are characterized by changes in lattice parameter via X-ray Diffraction (XRD), micro-hardness via nanoindentation, and the presence of a secondary phase imaged via Transmission electron microscopy (TEM) technique.

Role of Stoichiometry on Ordering in Ni-Cr Alloys

by
Fei Teng

A THESIS

submitted to

Oregon State University

in partial fulfillment of
the requirements for the
degree of

Master of Science

Presented May 17, 2016

Commencement June 2016

Master of Science thesis of Fei Teng presented on May 17, 2016.

APPROVED:

Major Professor, representing Materials Science

Director of the Materials Science Program

Dean of the Graduate School

In understand that my thesis will become part of the permanent collection of Oregon State University libraries. My signature below authorizes release of my thesis to any reader upon request.

Fei Teng, Author

ACKNOWLEDGEMENTS

There are many people who have contribution to my research. I wish to expresses sincere appreciation to them here. First, I would like to express my very profound gratitude to my academic advisor, Prof. Julie Tucker, for guiding me to the research topic, extending my academic horizon by sending me to academic conferences, and support throughout my graduate career. Her wisdom on research and patience on improving my English have helped me to better understand this research field and play an invaluable role in my way to graduation.

Then I wish to acknowledge Dr. Brady Gibbons and Dr. David Cann for their helpful suggestions in both XRD experiments and data analysis. I would also like to thank Dr. Troy Ansell for giving me training and enlightenment on XRD. I wish to extend my sincere appreciation to Dr. Melissa Santala for giving great help on getting darkfield image and performing duel-beam condition in TEM. I would like to thank Dr. Peter Eschbach for giving me training and assistance on FIB and TEM as well. Their great patience and academic experience play an irreplaceable role in my TEM skill.

I also wish to thank my colleagues in Nuclear Material and Metallurgy group at the Oregon State University. I would like to thank Mr. Cody Fast for giving me training on nanoindentation and data analysis. His hands-on experience and suggestions largely reduce my beginning time on nanoindenter. As a foreign student, I wish to acknowledge Mr. David Garfinkel, Lucas Teeter, and Ian Love for giving me helpful suggestions on my presentations and articles. Their patience and enthusiasm on improving my English has supported me on my way to a Master’s degree and life in US.

Finally, I would give appreciation to my parents, Kai Teng and Fengmei Liu. I cannot stand here as a graduate student and be able to seek future Ph.D. without your endless and unconditional love. Your words accompany me every school day and takes me through every lonely library night. I love you forever and I will always be with you.

TABLE OF CONTENTS

TABLE OF CONTENTS (Continued)

TABLE OF CONTENTS (Continued)

LIST OF FIGURES

LIST OF FIGURES (Continued)

<u>Figure</u> <u>Page</u>

LIST OF FIGURES (Continued)

Figure Page

LIST OF TABLES (Continued)

To my parents

滕凯 刘凤梅

1 Chapter 1 - Introduction

Light water reactors (LWR) are widely used in the power generation industry. The primary limitation of reactor lifetimes comes from environmental degradation of reactor components, due to radiation damage, corrosion, and high temperature phase transformation, which change mechanical properties with time. Considering the complicated environmental factors in reactors, some key components such as reactor pressure vessel heads and steam generators are difficult and costly to replace, which makes the component lifetime extension an important role in reactor plant license renewal and safety evaluation. Considering the harsh service environment, nickel-based alloys are widely used in nuclear plants because of their excellent corrosion resistance, fracture toughness, and stable metallic properties after ageing. Among key components, steam generator tubing (shown in Figure 1.1), which connects primary and secondary coolant cycles, reactor pressure vessel heads, and control rod drive mechanism penetrations are the primary components that are now being made with nickel-based alloys.

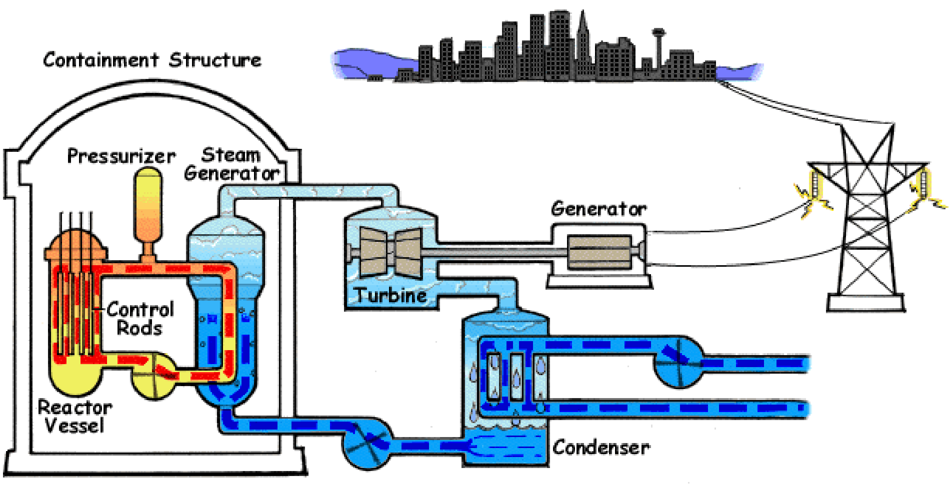

Figure 1.1 The overview of PWR and the role of stream generator [1].

Considering a service environment of relatively high temperatures (~300℃) and long lifetimes, Ni-based alloys, such as Inconel 690 and 625, are usually used in these core components of power plant. The ratio of Ni/Cr of these commercial alloys is located in ordering phase transformation field in phase diagram (from 0.65~0.7 Ni% Figure 1.2). During the transformation, atoms rearrange from random solid solution into regular patterns (layers of Ni and Cr) below a critical temperature, T_c. Ordering occurs when the attractive force between different atoms is larger than that of same atoms. If the alloy is near the stoichiometric compositions, the ordered phase will nucleate and grow [2]. The main objective of this project is to optimize the use of nickel-based alloys by studying the role of stoichiometry on the rate of ordering. To accomplish this goal, several Ni-Cr binary model alloys with different compositions are isothermally aged and characterized to determine the range of thermal embrittlement susceptibility.

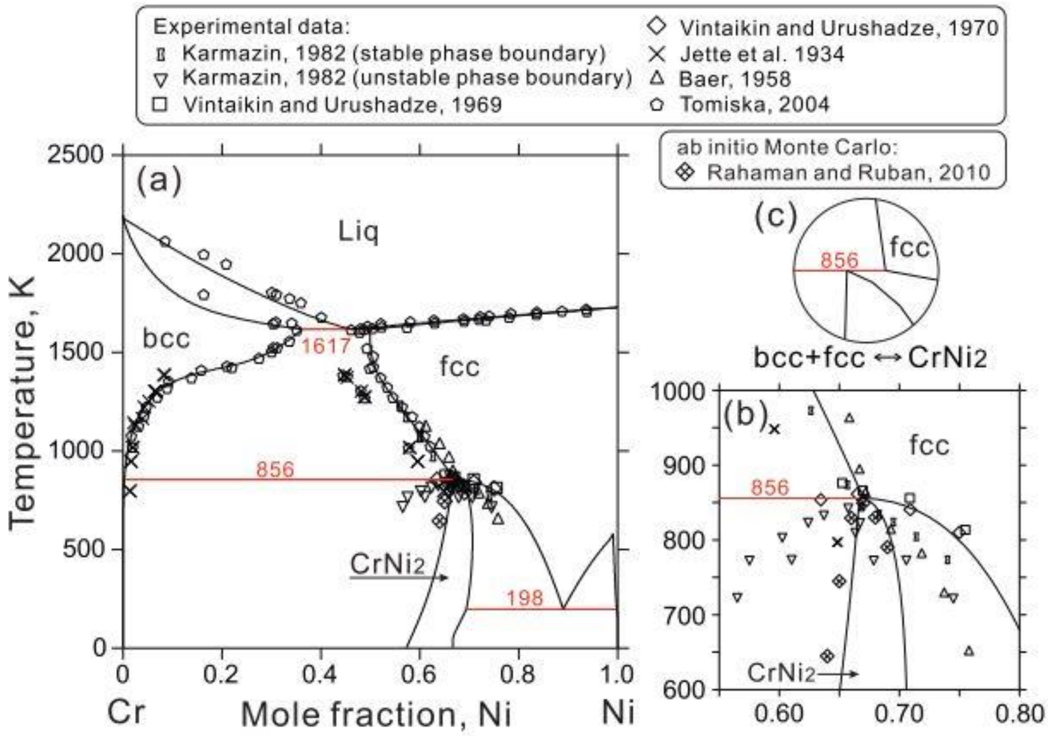

Figure 1.2 Comparison of the Cr-Ni phase diagram according to thermodynamic modeling in most current work in 2012 [3].

Figure 1.2 shows the most recently evaluated Ni-Cr phase diagram, which includes data below 500℃ (773K) [3]. In this project, four compositions are selected for isothermal ageing: 63.4%Cr, 58.9%Cr, 54.9%Cr, and 52.6%Cr, which corresponds to the Ni/Cr ratios: 1.8, 2.0, 2.2, and 2.4. The choice of composition is based on several commercial alloys. Table 1.1 shows the compositions of several commercial Ni-Cr alloys [4]. Different alloying elements affect the ordering behavior and the corresponding ageing behaviors, however, it is the ratio of Ni-Cr that is the focus of this thesis.

Table 1.1 Chemical composition of some commercial Ni-Cr based alloys (wt%) [4].

Alloy	C	Si	Mn	Cr	Fe	Ni	Ti	Al	Nb	Mo	Co	TnO_2
Brightray's	0.030	0.15	0.04	20.00	0.02	79.39	0.34	0.10	--	--	--	--
T.D. Ni Cr	0.006	0.003	--	19.20	--	78.70	--	--	--	--	--	2.01
Nimonic 75	0.120	0.53	0.45	19.40	4.28	72.35	0.36	0.13	0.05	0.07	0.42	--
Nimonic 80A	0.080	0.27	0.14	19.50	0.81	75.32	2.40	1.41	--	--	--	--
Nimonic PE16	0.051	0.19	0.08	16.26	33.97	43.40	1.14	1.28	--	3.25	0.24	--
Inconel X-750	0.030	0.23	0.23	14.89	6.46	73.93	2.50	0.74	0.93	--	--	--
Inconel 690	0.010	0.43	0.33	29.20	8.85	60.46	0.26	0.26	--	0.03	0.03	--
Sanicro 71	0.053	0.26	0.79	15.60	9.40	72.70	--	--	--	--	--	--
20Cr-25Ni st.	0.022	0.59	0.77	19.80	53.71	25.05	0.01	0.01	0.60	--	0.04	--

To eliminate other complicated environmental effects and to clarify effect of heat treatment on ordering, isothermal ageing is performed on all binary alloys at three different temperatures: 373℃, 418℃, and 475℃. All testing temperatures and compositions are located in $CrNi_2$ phase regime in Figure 1.2. After isothermal ageing, material characterization needs to be performed on samples, such as X-ray diffraction (XRD) for measuring the lattice parameter, micro-hardness for measuring hardness, which corresponds to embrittlement, and transmission electrical microscopy (TEM) for identifying the existing of ordering phase.

2 Chapter 2 - Literature Review

2.1 Abstract

Under long time service at elevated temperature, which is below 550℃, Ni-Cr based alloys can undergo an ordering phase transformation and develop short-range ordering (SRO). The short-range ordered structure can develop into long-range order (LRO) with time. Composition plays an important role in the transformation and alloys near the Ni_2Cr stoichiometry are at risk.

The short-range and long-range ordering transformation in Ni-Cr alloys has three consequences. First, the lattice parameter will contract and the contraction causes dimensional instability, resulting in “negative creep” or material contraction under load can be seen in the material after aging. Second, the ordered structure changes electrical and thermal properties of material. Third, pile ups of dislocation dipoles and the slip character changes from homogeneous to heterogeneous in way of promoting planar slip along [2]. Both can influence the mechanical properties, such as increasing the yield stress and decreasing the ductility, environmentally assisted cracking resistance of face centered cubic (FCC) alloys and promoting brittle, intergranular fracture [5].

Because of these consequences, the transformation between disordered and ordered phases can be identified by monitoring the variations in lattice parameter, electrical resistivity and micro-hardness.

2.2 Order-Disordered Transformation

Ordering is defined as atomic rearrangement, in regular patterns, which occurs below a sharply defined critical temperature, T_c [2]. The Ni_2Cr structure, which is shown in Figure 2.1, is a $MoPt_2$ prototype in *Immm* space group. The 001 direction in Figure 2.1 corresponds to the [110] in the FCC cell. In Figure 2.1, Cr atoms are in rust color and Ni atoms are in silver, which shows arrangement of Ni and Cr map in

FCC crystal structure [6]. The critical temperature depends on composition with a peak at the Ni_2Cr stoichiometry. Older Ni-Cr phase diagrams from Nash [7] only includes the data above 500℃. More recent research result shows the phase diagram and comparison between experimental and simulated result below 500℃ [3] (see Figure 1.2). New results show that the $MoPt_2$ structure can only be formed below ~856K (~583℃) and in a narrow composition range (65 to 71 at% Ni, which corresponds to $\frac{Ni}{Cr} = 1.8\ to\ 2.4$).

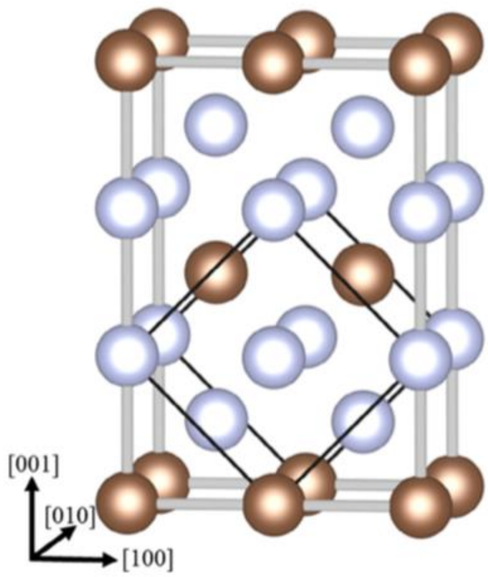

Figure 2.1 $MoPt_2$ prototype ordered structure in Ni_2Cr stoichiometry binary model alloy [8].

In most situations, ordering occurs by way of nucleation and growth, which means the growth rate is controlled by both rate of nucleation, in high temperature region, and rate of growth, in low temperature region. Consequently, C-curve kinetics of transformation shows in the relationship between ordering and temperature. The peak ordering rate temperature is about 475℃ for Ni-Cr binary alloys [5].

2.3 Kinetics of Order-Disorder Transformations

2.3.1 Short-range Ordering (SRO)

Short-range ordering (SRO) means that statistical probability of finding different species as a next-nearest neighbor atoms may be higher than that in random solution. SRO has critical requirements; 1) the temperature must be below T_c and 2) the composition must be near stoichiometric composition such as AB, A_2B, A_3B, etc. The T_c in an off-stoichiometric alloy will be lower than that of stoichiometric material [2]. In Ni-Cr alloys, the degree of SRO decreases with decreasing temperature, increases with increasing Ni concentration, and decreases with decreasing Fe concentration [2].

SRO can occur in the matrix at the early stage of aging (a few hours, [9]), during slow cooling, by annealing after quenching, by deformation or neutron irradiation. SRO consists of a dispersion of tiny zones with a dimension of a couple of nanometers in disordered matrix [10]. The SRO state is accompanied by an increase in resistivity and a negligible effect on hardness [9]. SRO can also occur during cold work at lower temperature, because the large amount of defects increases the rate of diffusion.

2.3.2 *Long-range Ordering (LRO)*

The degree and kinetics of LRO depend on the aging conditions. The barrier to further growth of SRO regions into LRO is lowered by aging below a critical temperature. Ordering kinetics can be accelerated by furnace cooling from high temperatures, applied elastic stress, the presence of excess vacancies (e.g., from quenching or irradiation) and some alloying additions. LRO kinetics can be delayed by cold work in way of destroying initial ordered regime. Cold work can also raise apparent activation energy, which means that ordering rate is decreased compared to un-cold worked alloys [5]. On the contrary to SRO, LRO increases hardness compared to the disordered state [9]. The lattice contraction associated with LRO causes internal stress, which approaches the alloys yield strength under constant strain [5]. LRO can be identified by lattice parameter contraction because the effective lattice change upon complete long range ordering is about ~0.25%. LRO can produce significantly stress and dimensional changes, such as negative creep, in material [2].

The lattice parameter and microhardness changes can be described by Kolmogorov-Johnson-Mehl-Avrami (KJMA) equation (equations 1 & 2):

$$f = (1 - e^{-(kt)^n}) \tag{1}$$

$$k = k_0 e^{-Q/RT} \tag{2}$$

$$f = \frac{H - H_0}{H_{Max} - H_0} \quad \text{for microhardness, or} \tag{3}$$

$$f = \frac{a_0 - a}{a_0 - a_{Min}} \quad \text{for x-ray diffraction} \tag{4}$$

where f is the fraction transformed, t is the aging time, n is the Avrami exponent, k_0 is the pre-exponential factor, Q is the apparent activation energy, R is the gas constant, and T is the aging temperature [11-15]. For LRO, previous studies have found that Q limited by vacancy migration (~135kJ/mol) and bulk diffusion (~275kJ/mol) and the value n is between 0.5 and 1.5, usually n=1, indicative the growth of ordered phase controlled by diffusion [8]. This model assumes that the lattice parameter changes or hardness change is directly proportional to the phase fraction transformed.

2.4 Ordering Transformation in the Ni-Cr-Fe System

In Ni-Cr-Fe ternary system, SRO in matrix phase can transform to LRO phase, which is of the Ni_2Cr ordered structure, when exposed to temperatures between 425 to

475°C (depending on the Fe composition). In some cases, over 30,000 hours are required to achieve completed transformation depends on addition of Fe (Figure 2.2) [9]. A study by Marucco also shows that transformation kinetics in stoichiometric alloys is far more rapid than that in off-stoichiometric alloys. In other words, the degree of LRO decreased as the deviation from stoichiometry increases [9].

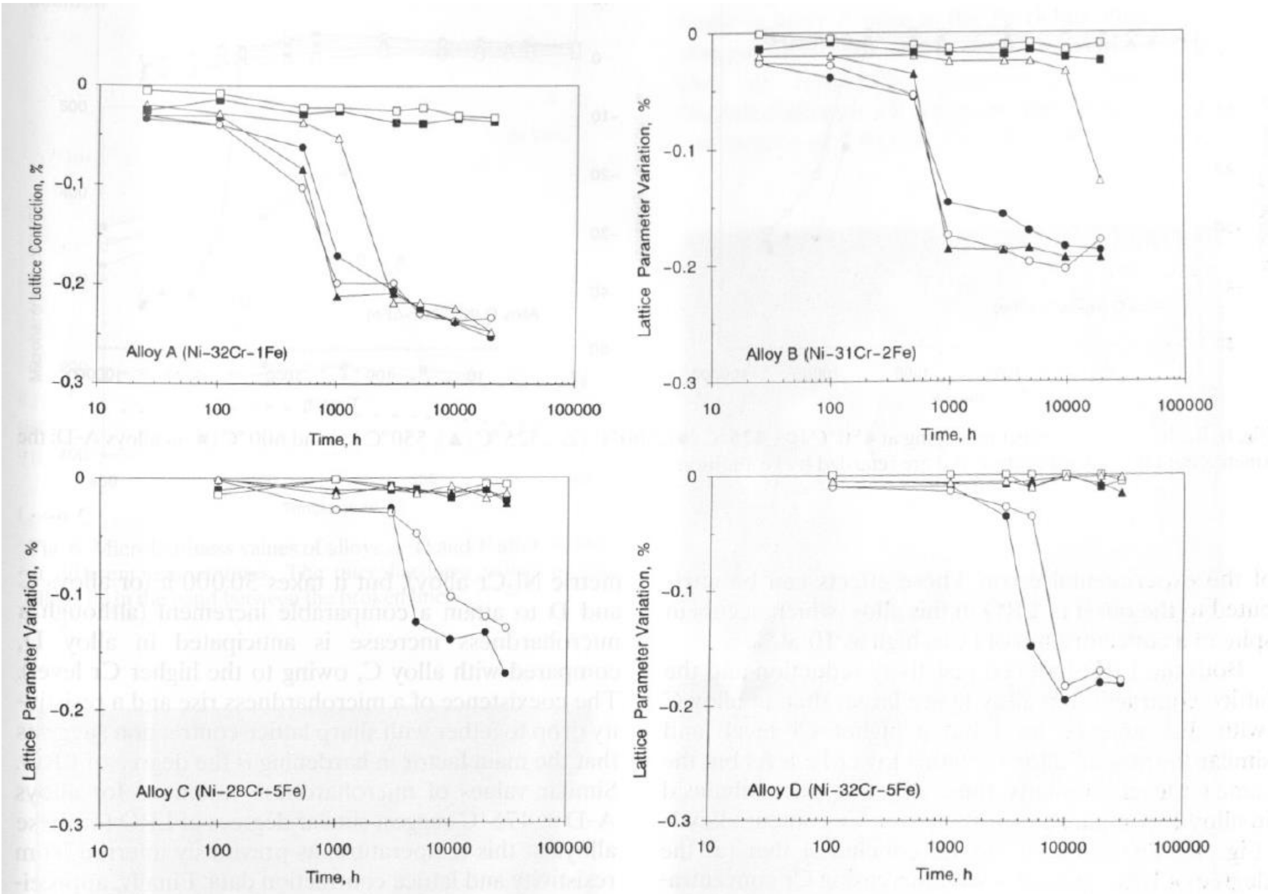

Fig. 5. Lattice contractions upon aging at 450 °C (○), 475 °C (●), 500 °C (△), 525 °C (▲), 550 °C (□) and 600 °C (■) in alloys A–D: the kinetics depend on temperature and are retarded by Fe addition.

Figure 2.2 Ordering transformation of alloys with different compositions.

To understand the mechanism of ordering in Ni-Cr commercial alloys, studies on transformation between SRO to LRO on Ni_2Cr superlattice structure are extracted out and simplified on binary alloys, Ni_2Cr and Ni_3Cr. For ordered Ni_3Cr in Ni-Cr-Fe system, an increase in resistivity, which means SRO, is shown after 24 hours aging and remains constant for up to 25,000 hours. For ordered Ni_2Cr in Ni-Cr-Fe system, which has the maximum kinetics composition, the early stage is similar to Ni_3Cr, which means the SRO begins to transfer to LRO after a few hundred hours aging and SRO does not disappear suddenly when T_c is exceeded but vanishes gradually. T_c depends on composition and varies between 530 and 580℃. The transformation can be confirmed by Ni_2Cr superlattice reflection in electron diffraction pattern and the decrease in resistivity [10].

In Ni-Cr-Fe ternary system, the LRO is hard to define because Fe content in excess of 7 at% will inhibit or delay its formation. For a series of alloys with the composition shown below (Table 2.1), the result, which is shown in Figure 2.3, shows that the degree of LRO, which can be related to variations in lattice parameter, resistivity, and micro-hardness, shows that the degree of LRO increases with Cr level. LRO can be significantly delayed by additional Fe [9].

Table 2.1 Composition of samples in Ni-Cr-Fe system [9].

Alloy	**A**	**B**	**C**	**D**	**E**	**F**	**G**	**H**	**I**	**J**	**K**
Ni (at%)	66.5	66.4	66.4	63.0	66.3	59.3	67.0	52.9	46.0	39.9	30.8
Fe (at%)	1.1	2.1	5.1	5.2	10.2	10.4	15.4	20.4	29.8	40.5	51.4
Cr (at%)	32.4	31.5	28.4	31.7	23.4	30.2	17.4	26.7	24.0	19.5	17.8
Ni/Cr	2.05	2.1	2.34	1.99	2.83	1.96	3.85	1.98	1.92	2.05	1.73

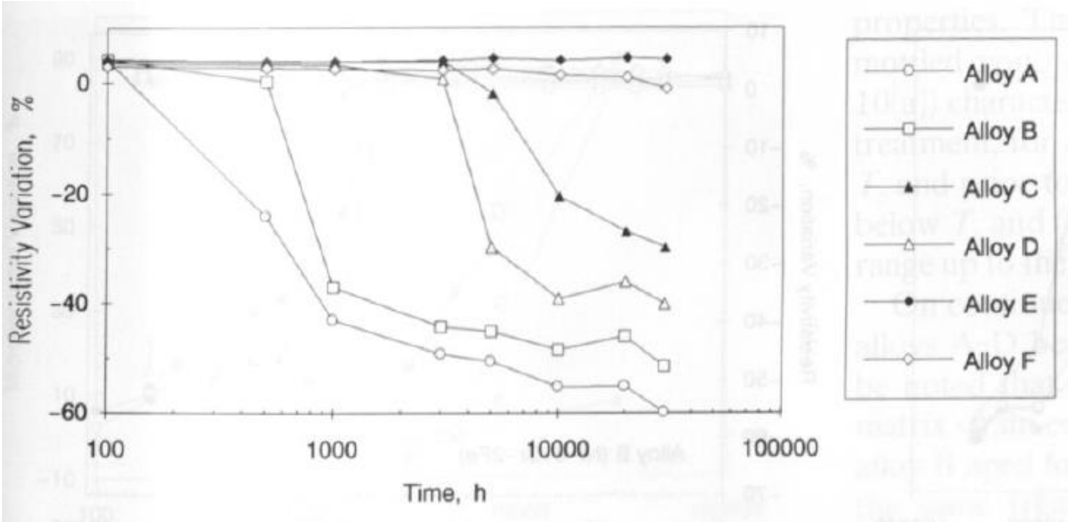

Figure 2.3 LRO-induced resistivity variation at 475℃ in alloys with up to 10 at.% Fe [9].

Fe concentration also influences the degree of SRO in ternary system. $Ni_2(Cr,Fe)$ type phase have higher resistivity value than Ni_2Cr+Fe type phase. $Ni_2(Cr,Fe)$ phase is caused by substitution of Cr by Fe in Ni_2Cr lattice. Ni_2Cr+Fe type phase is caused by Ni_2Cr precipitates in a Fe-rich matrix phase. In commercial Ni-based super alloy system, the compositions of all the investigated alloys are shown in below table. The result shows that SRO forms in all the alloys [4].

Iron will increase plateau of resistivity versus time and lowers ordering rate, but the ordered phase can still be observed under electron diffraction even in 10% iron alloy [9]. However, the rule does not work in both industrial 690 alloys. LRO can be observed in 690 model alloy $(Ni_{0.67}Cr_{0.33})_{1-x}Fe_x$ under irradiation [16]. However, no LRO transformation is observed in 690 commercial alloy even with high of a High Voltage Electron Microscopy [17]. More details will be mentioned in "Role of Irradiation on Ordering" section.

Table 2.2 Chemical composition of some commercial Ni-Cr based alloys [4].

Alloy	Cr	Fe	Ni	Ni/Cr
Brightray's	20.00	0.02	79.39	3.97
T.D.Ni Cr	19.20	--	78.70	4.10
Nimonic 75	19.40	4.28	72.35	3.73
Nimonic 80A	19.50	0.81	75.32	3.86
Nimonic PE16	16.26	33.97	43.40	2.67
Inconel X-750	14.89	6.46	73.93	4.97
Inconel 625	20-23	5.00 max	58.00	~2.52
Inconel 690	29.20	8.85	60.46	2.07
Sanicro 71	15.60	9.40	72.70	4.66
20Cr-25Ni st.	19.80	53.17	25.05	1.27

2.5 K-state

The initial resistivity plateau behavior is known as “K-state”. The state is characterized by “increase in electrical resistivity on aging as compared to the quenched state” [2], which is shown in Figure 2.4. K-state behavior can be used as an assistant method with XRD to confirm LRO transformation. For K-state alloys, cold-work decrease resistivity, conflicting with the normal behavior of alloys and metals [18]. The reason of plateau is that ordering domains begin to impinge on each other with ordering transformation in progress [2].

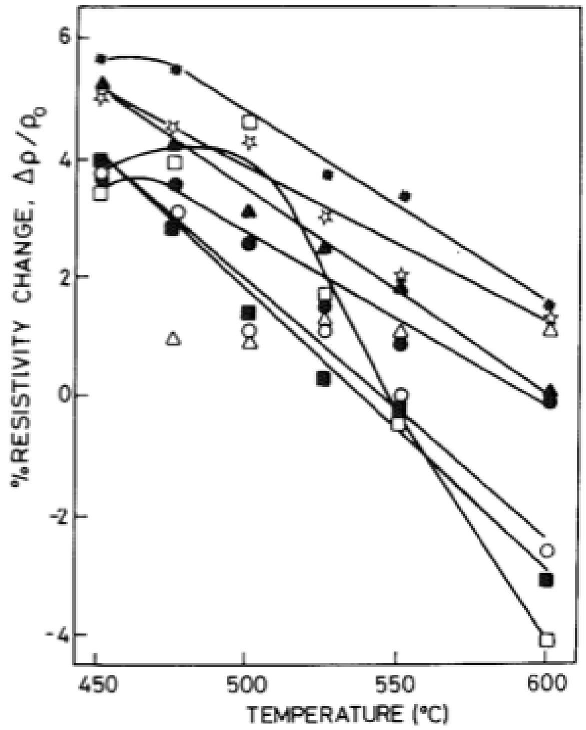

Figure 2.4 The K-state effect on resistivities of some commercial Ni-Cr alloys after 1000 hrs aging at 475℃. *(○) Brightray "S", (□) Nimonic 80A, (Δ) 20Cr/25Ni Steel, (*) Sanicro 71, (●) Inconel 690, (■) Inconel X750, (▲) Nimonic 75, (⋆) TD NiCr* [2].

K-state alloys can be made in way of either quenching from high temperature or cold-work and then aged at low temperature when the alloy composition is similar to that of an ordered phase [2].

There are four conclusions about K-state based on study of anomalous isochronal resistivity curves. First, resistivity increasing upon aging due to nucleation and growth of ordered phase. Second, furnace-cooled samples don't have K-state, because of the completed SRO before aging. Then, resistivity of water-quenched samples is lower than that of furnace-cooled ones. Finally, cold working destructs SRO and leads to decrease in resistivity [2].

2.6 Effect of Ordering on Mechanical Properties

Ordered phases influence mechanical properties by changing the dislocation morphology of material from homogeneous to heterogeneous planar slip. Current result fromYoung, Figure 2.5, shows that the ordered phase has embrittlement effect on the stress-strain behavior [5]. The changing of dislocation morphology decides the hardening coefficient and temperature, which is shown in Figure 2.6. A behavior, which is known as heterogeneous dislocation, occurs in the ordered phase. When pile-up of dislocations forms, slipping on this plane will be restricted and other slipping planes will be activated, which will cause strain hardening [2].

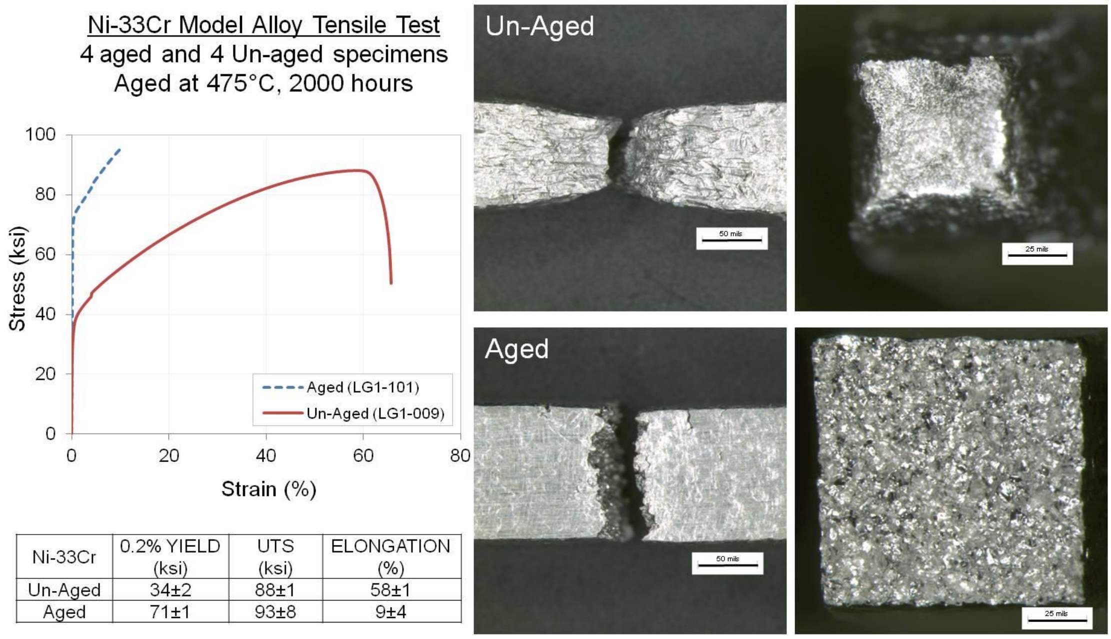

Ni-33Cr	0.2% YIELD (ksi)	UTS (ksi)	ELONGATION (%)
Un-Aged	34±2	88±1	58±1
Aged	71±1	93±8	9±4

Figure 2.5 Ni-33Cr model alloy tensile test 4 aged and 4 un-aged specimens. Aged at 475°C, 2000 hours [5].

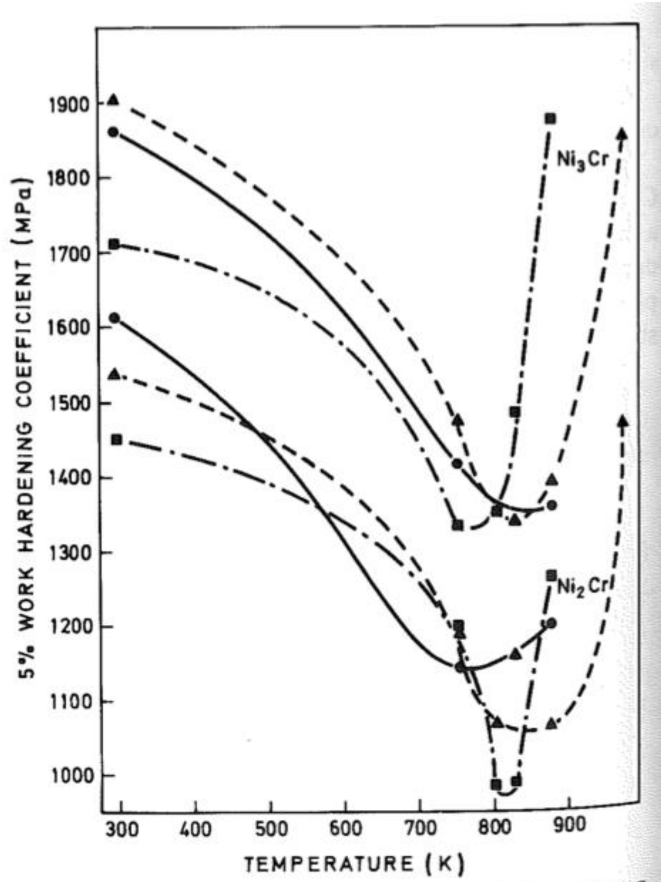

Figure 10 The work hardening coefficient of Ni_2Cr and Ni_3Cr at different temperatures and strain rates. (–●–) $2.33 \times 10^{-4} sec^{-1}$, (– – ▲ – –) $8.33 \times 10^{-5} sec^{-1}$, (· – ■ – ·) $1.17 \times 10^{-6} sec^{-1}$.

Figure 2.6. The hardening coefficient of Ni_2Cr and Ni_3Cr on different temperature and strain rates [2].

2.7 Role of Irradiation on Ordering

The topic of irradiation effect in Ni-Cr-Fe has been explored by Frely who used electron irradiation to accelerate the ordering rate [16, 19]. The influence of irradiation on ordering may be different depending on temperature. Irradiation can have two opposite effect on the ordering transformation. One is that irradiation will enhance ordering at intermediate temperatures, which happens when radiation defects are mobile and their concentration is much higher than that of thermal defects. The other effect is that ordering can be reduced by defects produced by collision, when irradiated with high energy particles. This is the primary influence on ordering at low temperature because of the relative fixed position of defects.

The ordering kinetics from the research of Frely includes following results: first, the plateau of kinetics under irradiation is shorter than that of thermal ordering kinetics, which means the resistivity decreases faster under irradiation and the initial increasing in resistivity is similar to SRO [16] (Figure 2.7). Second, adding iron usually increases the length of plateau and decreases the ordering rate, which makes the ordered phase harder to see. The ordered phase can be observed via electron diffraction pattern under TEM even in the 10% iron containing alloy. Third, under low flux of the Van de Graaff accelerator or high flux of a High Voltage Electron Microscope (HVEM), no industrial alloy showed any long range ordering, but model 690 did show ordering, which suggests that minor alloying may play a role in ordering kinetics. However, theexistence of the ordered phase has been confirmed in 690 commercial alloy by others [17] Fourth, cold-rolling increases the dislocation density, which helps to eliminate irradiation defects, and decreases the ordering rate by lowering diffusion. However, this effect is not strong enough to explain no ordering in industrial alloys. Fifth, irradiation decreases the optimum temperature of ordering from about 500℃ to 400℃. Decreasing of optimum temperature is caused by the diffusion ability, which means mobility increases, as the result of irradiation [16].

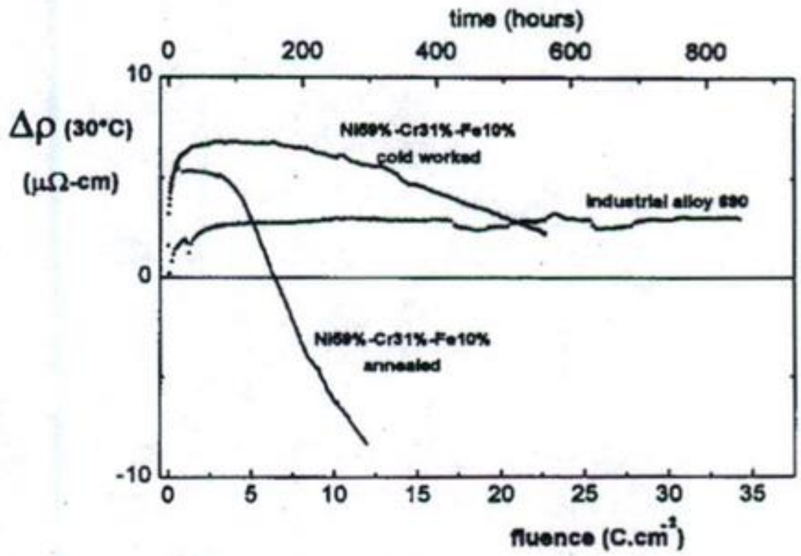

Figure 2.7 Resistivity variation versus irradiation fluence (or time) for the industrial alloys and the model alloy, annealed or cold worked (the fluctuations due to electron beam instabilities) [16].

2.8 Characterization Ordering by X-ray Diffraction (XRD)

X-ray diffraction can be used to calculate the lattice parameters before and after ageing due to the contraction caused by ordering. As mentioning in section 2.3.2, the critical value of lattice contraction is ~0.25% [2], which means the samples need to be prepared carefully to keep high precision in order to detect this small change. To fulfill the request, the aged samples are ground to remove oxide and metallographically prepared. Electropolishing is typically used to eliminate the influence of grinding, or work-hardening effect. Parallel beam optics and high angle, which are about 140° and 150°, are used to minimize the error from instrument [5, 20].

In the research of Marucco [4], lattice contraction behavior of Ni_2Cr has been studied from 450℃ to 600℃, which is shown in Figure 2.8. The result shows that lattice contraction maxima happens from ~475℃ to 525℃. Longer ageing time leads to larger lattice contraction. In the research of Young [5], XRD has been used to explore the difference of water quench, furnace cool, and cold work in several binary and ternary model alloys. For water quenched Ni_2Cr model alloy, the result is shown in Figure 2.9. The result also shows that degree of ordering increases with increasing temperature when temperature is still below optimal temperature, which is ~500°C.

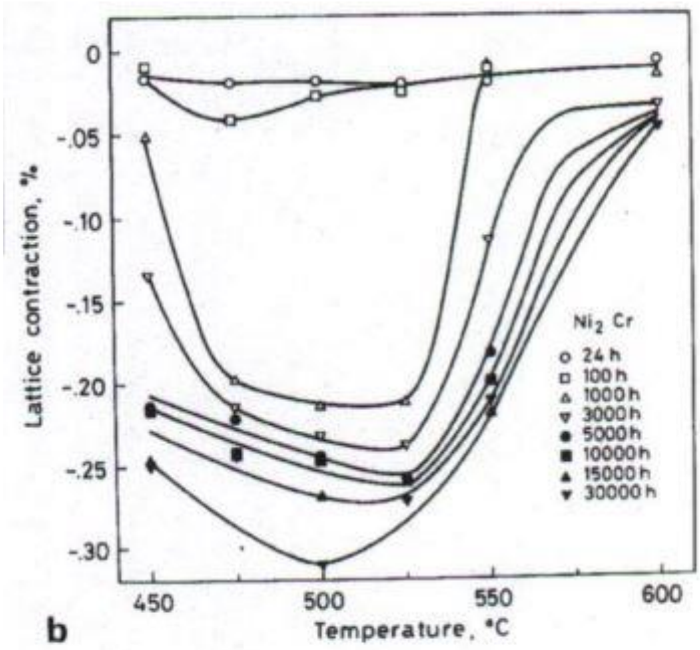

Figure 2.8 SRO- and LRO-induced lattice contraction in Ni_2Cr alloy [4].

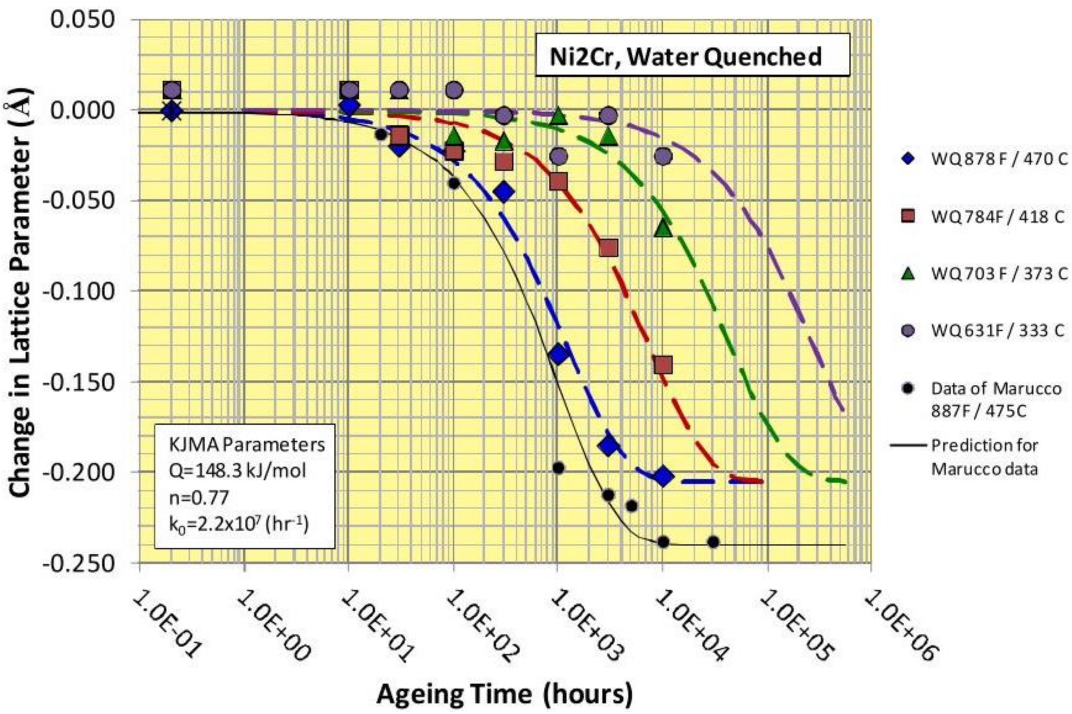

Figure 2.9 Comparison between simulation result and experimental result for water quenched Ni_2Cr via lattice contraction by XRD. [5]

2.9 Characterization via Transmission Electrical Microscopy (TEM)

Because of the effect of stoichiometry, ageing time, ageing temperature and other sample preparation conditions, the size of long range ordering domains can vary from several Angstroms (the bright spot phase shown in darkfield image in Figure 2.10) [18] to 2.3-3.2 nm (Figure 2.11) [21]. With enough time ageing, ordered domains can be visible under scanning electron microscopy (Figure 2.12) [4]. TEM, specifically diffraction pattern and dark field image, are used to characterize the formation of the long range ordering phase. When the ordered phase exists in significant phase fractions, secondary reflections, or superlattice reflections shall be apparent with the primary diffraction pattern from matrix phase.

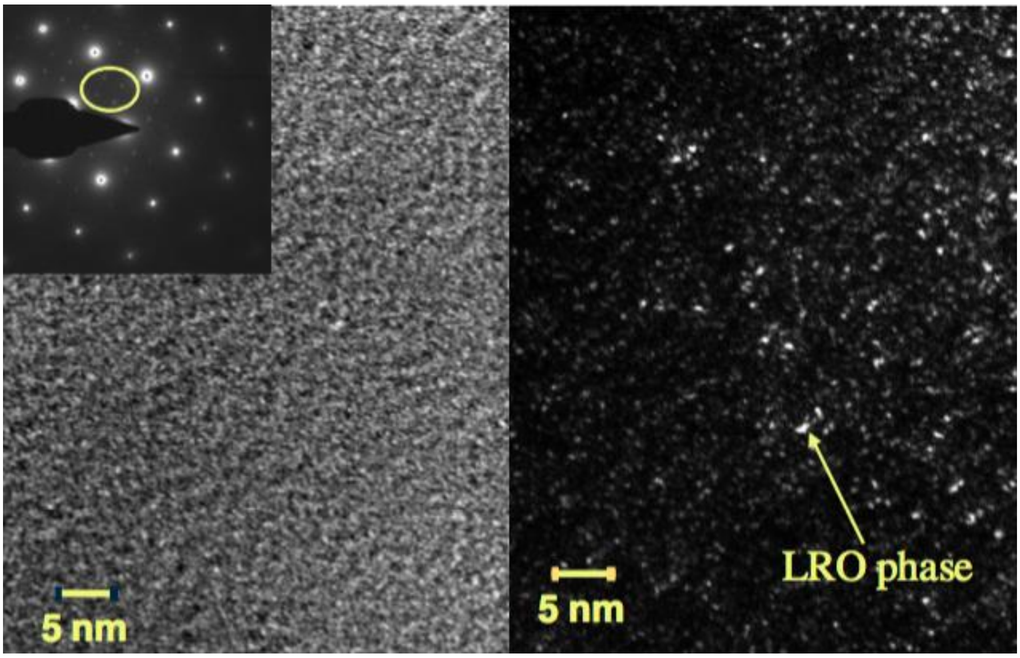

Figure 2.10 Dark field transmission electron microscopy and selected area diffraction patterns (Ni-Cr-3Fe alloy aged at 470℃ for 3,000 hours) [18].

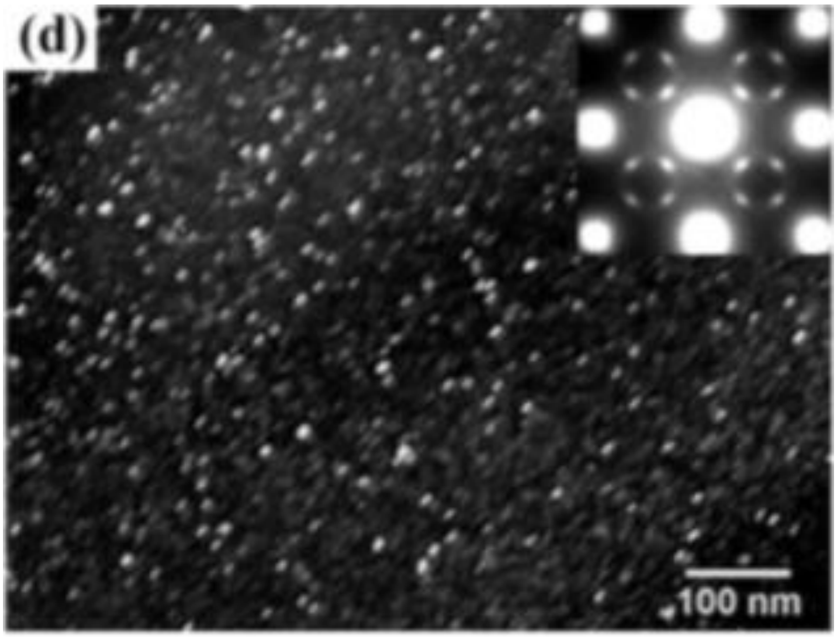

Figure 2.11. Darkfield transmission electron microscopy and selected area diffraction patterns ($Ni_2(Cr_{0.5}Mo_{0.5})$ alloy aged at 525℃ for 2 hours) [21].

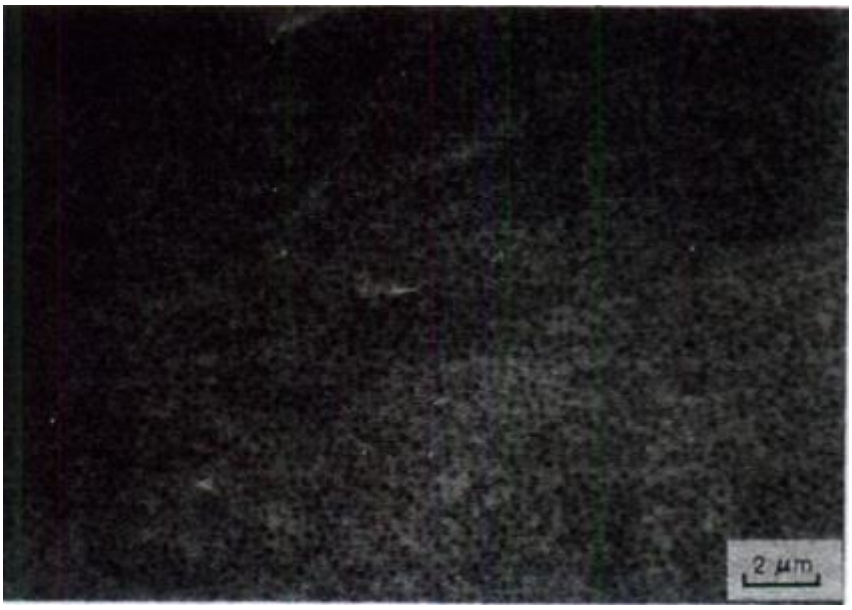

Figure 2.12. Scanning electron microscopy image, Ni_2Cr aged for 30,000 hours at 550°C: ordered domains in disordered matrix are observed [4].

3 Chapter 3 – Experimental Methods

3.1 Sample Preparation

Four binary Ni-Cr model alloys with different stoichiometry, $\frac{Ni}{Cr} = 1.8, 2.0, 2.2, 2.4$, are the focus of this study. The composition is confirmed by IMR Test Lab and the report is attached in Appendix A. Test method comes from CAP-017N (ICP-AES) and ASTM E 1019-11 (Comb./IGF), which are both mentioned in document. Both method describe the standard test methods for determination of C, S, N, and O in steel, Fe, Ni, and Co alloys by various combustion and fusion techniques. All samples were cut into small specimens with $10 * 10 * 5\ mm^3$ dimensions by electrical discharge machining (EDM) to avoid heating during cutting. Mechanical polishing has been used to remove oxide on the surfaces. First, 60 and 800 grit silicon carbide papers are used to remove most oxide. Then all samples are polished on polishing wheel with 0.5, 0.05, and 0.03μm aluminum oxide particle solution to prepare flat and shinning surface.

After polishing and before isothermal ageing, the lattice parameters of all samples were measured via XRD. After ageing, all samples are quenched in water to cool down to room temperature and sent to XRD to measure lattice parameters again without repolishing the sample surface.

3.2 Isothermal Heat Treatment

In this project, samples were given isothermal heat treatment at three temperatures as shown in test matrix (Table 3.1). To perform accurate research result, temperature must be controlled critically. Thermocouple measuring position should be located on sample stage instead the air around samples. Considering the measuring position of internal temperature monitoring system is air and the long time of the heat treatment, a new set of temperature monitoring and recording system with required accuracy and measuring position needed to be designed.

Table 3.1 Test Matrix of Isothermal Ageing

Time(hrs) **Temp(°C)**	**500**	**1000**	**3000**	**5000**	**10000**
475	1	1	1	1	2
418	1	1	1	1	2
373	1	1	1	1	2

3.2.1 System Design

The temperature monitoring system includes six parts: thermocouples, LabView program, National Instrument (NI) hardware, computer, data logger and calibration instruments for thermocouples. The data logger with thermocouples, which is independent from the computer with NI hardware, is used to record temperature if the computer system stops working. Setup of the system is shown in Figure 3.1 and Figure 3.2. The temperature of each furnace is measured by three thermocouples, two for LabView system and one for the data logger, which is independent from the computer. Temperature data is captured by thermocouples and the data is passed to computer via NI hardware. In the computer, the data is first stored in local hard drive, then it backups to cloud drive to keep the data safe in case of system issues in the computer such as crashing down and/or the program stopping for unknown reasons. The computer for data recording can be controlled remotely. Cloud drive can be visited by any computer as well.

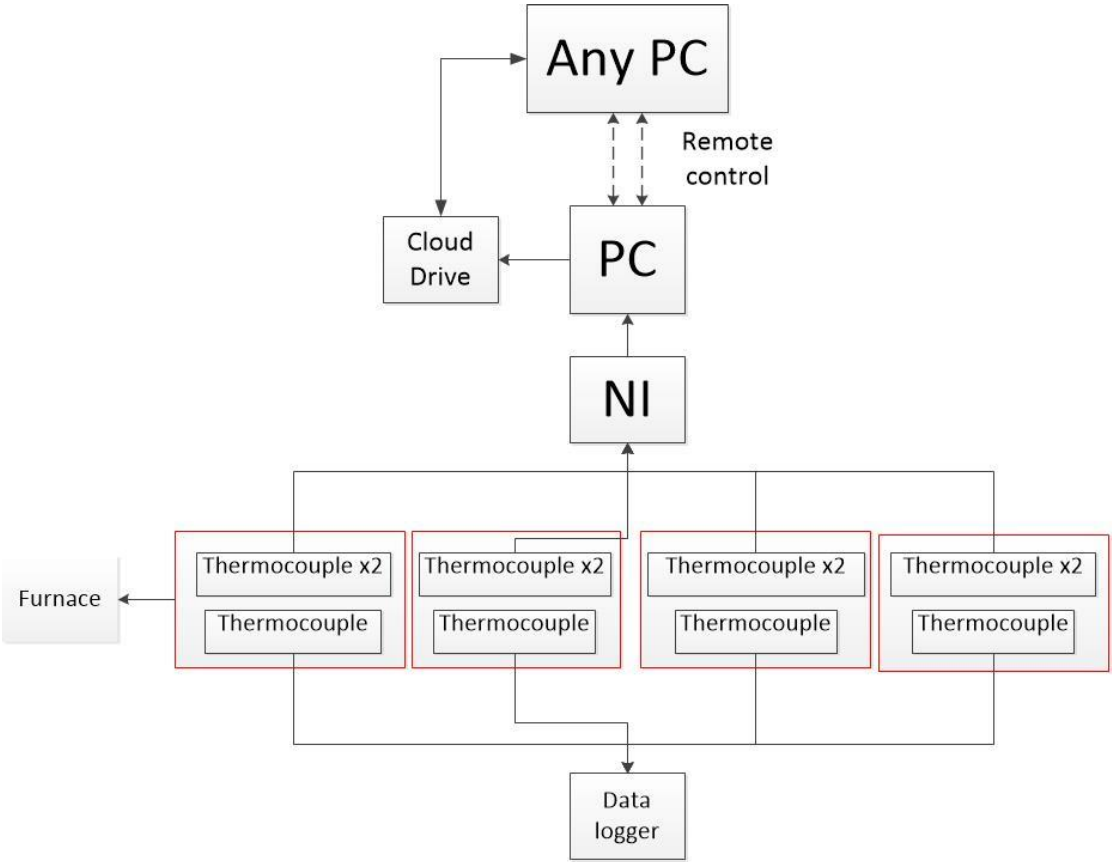

Figure 3.1 Setup of temperature monitoring system

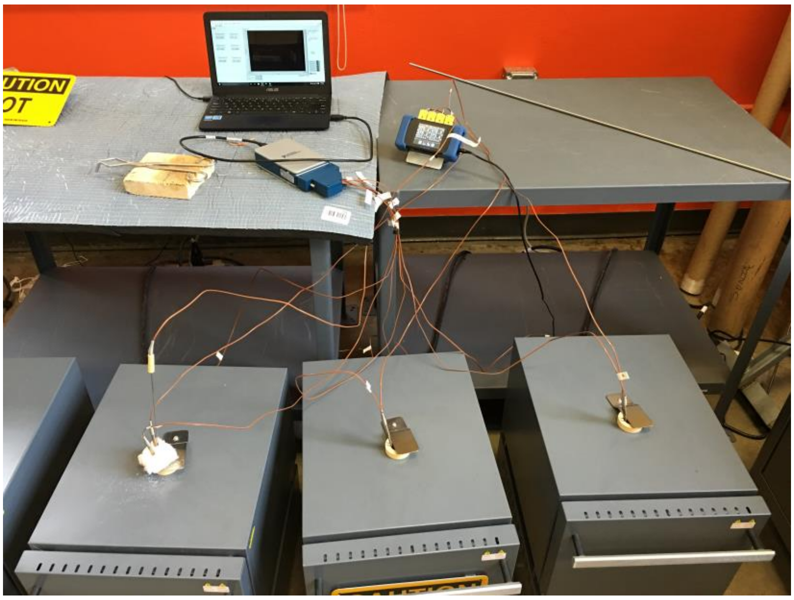

Figure 3.2 Arrangement of heat treatment system.

3.2.2 Thermocouple

Ungrounded type-K thermocouples are used in the isothermal heat treatment to keep accuracy of measuring during long time (Figure 3.3). In ungrounded thermocouples, wires are detached from probe wall (Figure 3.4), which has a higher accuracy and slower reaction speed because of the electron insulation offered by probe wall [22, 23]. Considering the measuring time is up to 10,000 hours, accuracy is of higher priority than reaction speed.

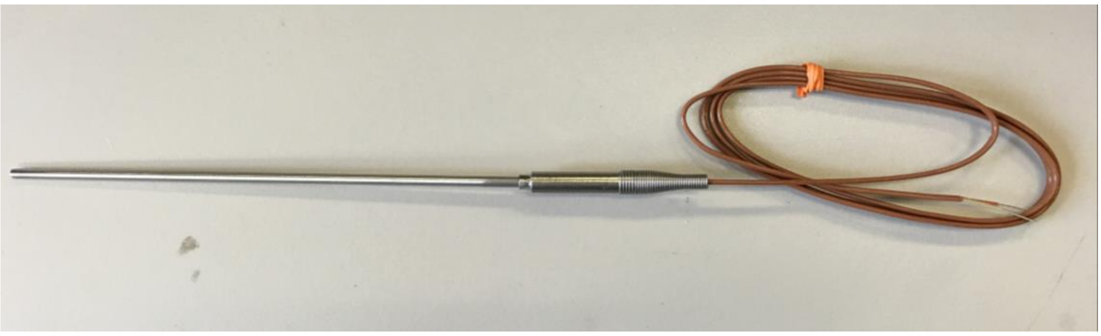

Figure 3.3 Ungrounded type-K thermocouple.

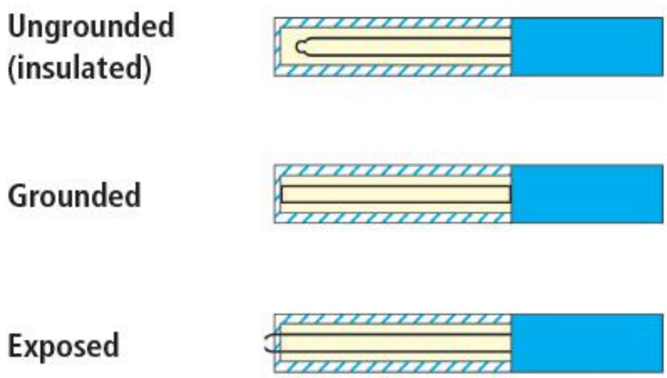

Figure 3.4 Internal Structure of ungrounded, grounded, and exposed thermocouple [23].

Figure 3.5 shows the position of samples, thermocouples, and sample stage. All thermocouples should attach ceramic sample stage and measure "solid temperature" instead of "air temperature."

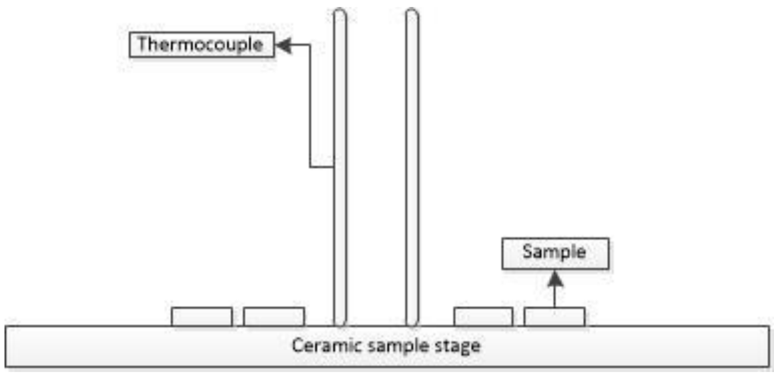

Figure 3.5 Sample and thermocouple measuring position in furnace.

3.2.3 LabView Program

Thermocouple measurements are passed to the NI hardware and recorded by a LabView program on the computer. Figure 3.6 is the layout of temperature monitoring program. Each furnace is monitored by two thermocouples to record different point on sample stage and in case of measurement drift in the thermocouples reading with ageing time.

Temperature data will be shown and recorded in the computer. A low temperature alert is also set in the system to send email alert to the user when the ageing temperature goes lower than a set temperature. Considering the tiny temperature vibration, the error to send email alert is 2℃ lower than setting temperature. Temperature data is recorded every 15 minutes.

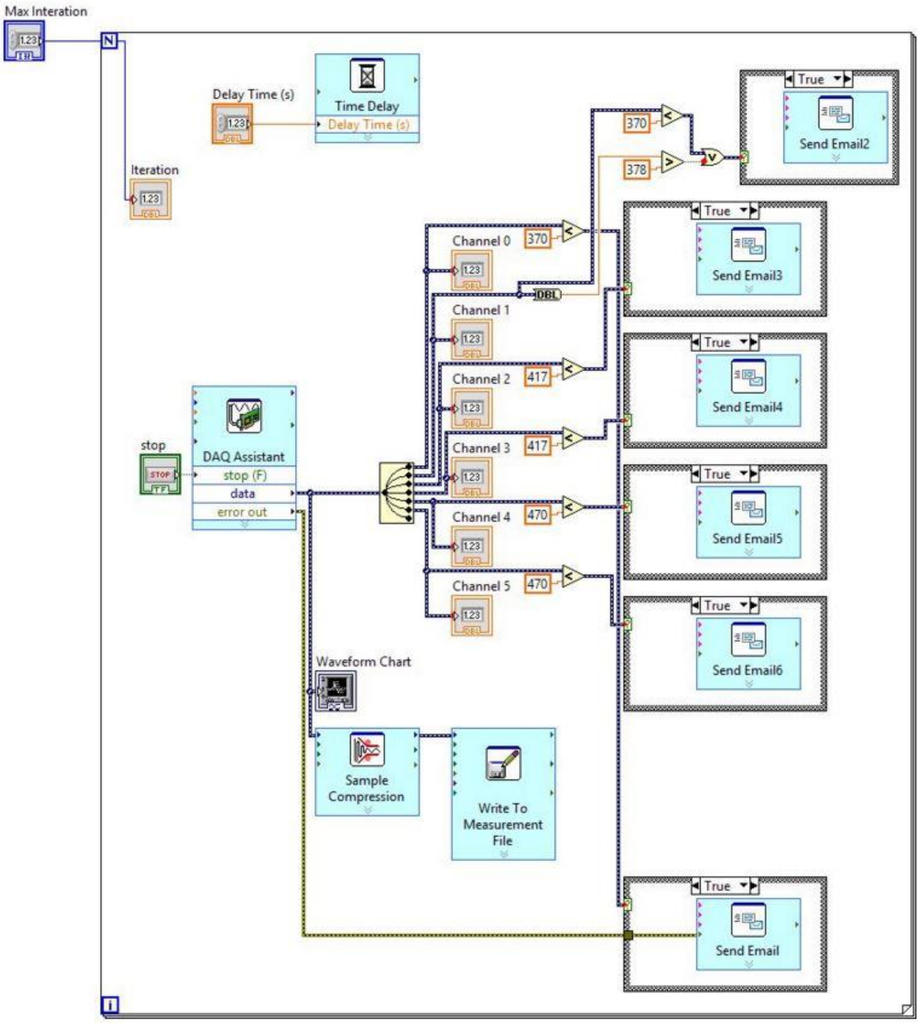

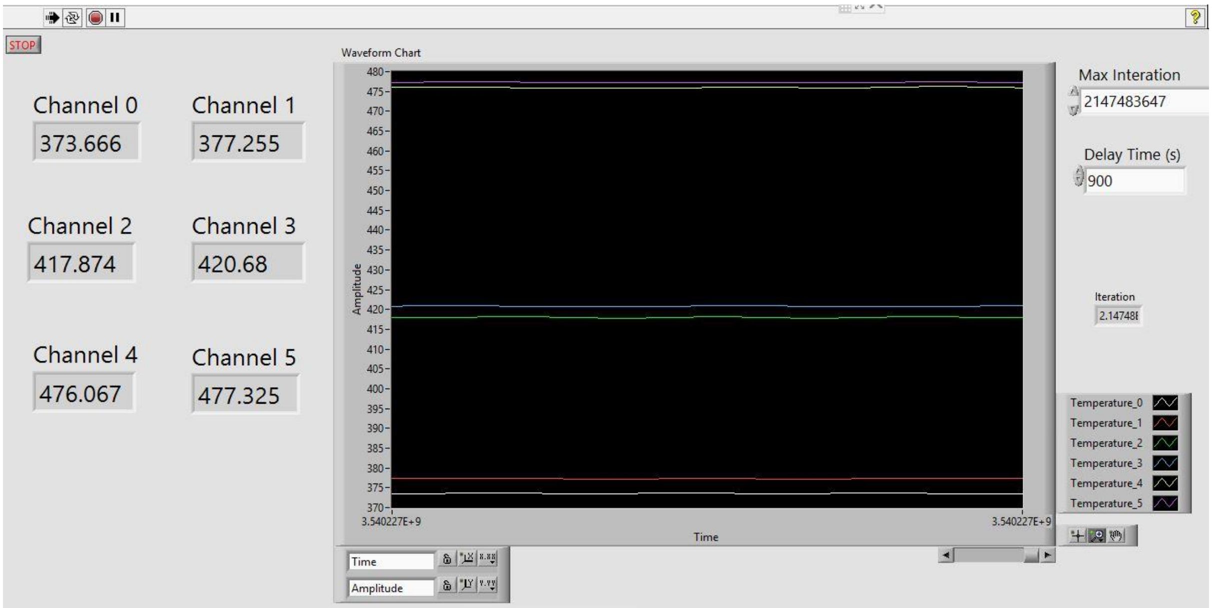

Figure 3.6 Layout (top) and front panel (bottom) of LabView Program.

3.2.4 Calibration of Thermocouples

Thermocouple properties may degrade over time with use. To ensure measurement accuracy, all thermocouples should be calibrated before using. Table 3.2 is a sample of a calibration table used for this experiment. The thermocouples with errors larger than ±2℃ will not be used. More calibration result are shown in Appendix B.

Table 3.2 Thermocouple calibration record.

Thermocouple Model:	KTSS-116U-12	
Thermocouple Type (i.e. J,K or T)	K	
Tag Number (TC-Type-Year-#)	Setpoint value [℃]	Deviation [℃]
TC-K-15-001	300	-0.18
	400	-0.04
	500	-0.40
	600	-0.92
Calibration date	09-02-2015	
Notes		

The instruments of calibration includes dry well tester (9144-A Field Metrology Well), 1502A Thermometer Readout (Figure 3.7), and 5609 Platinum Resistance Thermometer (Figure 3.8). Calibration procedures are shown in Appendix C.

Figure 3.7 Thermometer readout (left) & Calibration thermal well (right).

Figure 3.8 5609 Platinum Resistance Thermometer.

3.2.5 Temperature Record Data

Several points need to be noticed from temperature recording. First, the temperature difference between sample stage (solid temperature) and the air (air temperature) in furnace (Table 3.3). Considering samples are in contact with the ceramic sample stage, which is of larger heat capacity, thermal conduction is the predominant method of heat transfer. Second, consider the temperature variance between different seasons and different type of furnaces. Temperature stabilization is a result of dynamic balance between heating and dissipation. Considering these effect, the temperature of furnace needs to be adjusted for difference seasons and different types of furnaces to keep the real heat treatment temperature stable.

Table 3.3 Comparison between solid & air temperature in furnace.

Setting temperature (℃)	**Solid temperature (℃)**	**Air temperature (℃)**
373	373.5	377.3
418	417.9	420.8
475	475.9	477.3

3.3 X-ray Diffraction (XRD)

Base on previous research results [2], the disorder-order phase transformation observed in Ni-Cr alloys will result in lattice contraction, embrittlement and hardening. We can study the rate of ordering if we assume that these material property changes directly correlate to the phase transformation. In this section we will discuss results for changes in lattice contraction measured via XRD.

Previous studies on lattice contraction in Ni-Cr model alloys find the critical value of lattice contraction to identify long range ordering is ~0.25% [2, 5]. It is necessary to minimize both instrument measurement and sample preparation errors in order to obtain precise measurement of lattice parameter via XRD. The relationship between stoichiometry and lattice contraction after ageing will be shown here. The effect of polishing and etching, which are ways of removing surface oxide layer and releasing residual stress from mechanical polishing, on measuring lattice parameter will also be evaluated here.

3.3.1 XRD Result on Identifying LRO

Figure 3.9 is an example XRD plot from the $\frac{Ni}{Cr} = 2.0$ unaged sample (2.0-unaged for short in following). Five peaks can be identified from plot in range of 40° to 100° in step size of 0.014°, which occur near $44°, 51°, 75°, 92°,$ and 97°. The five peaks represent five corresponding planes: (111), (200), (220), (311), and (222). Considering the potential peak broadening due to phase transformation and the relative low intensity, which will make it difficult to precisely identify the peak angle, the (222) peak will not be used in the calculation of lattice parameter. Zero-background sample stage is used to eliminate noise peaks from the aluminum sample stage.

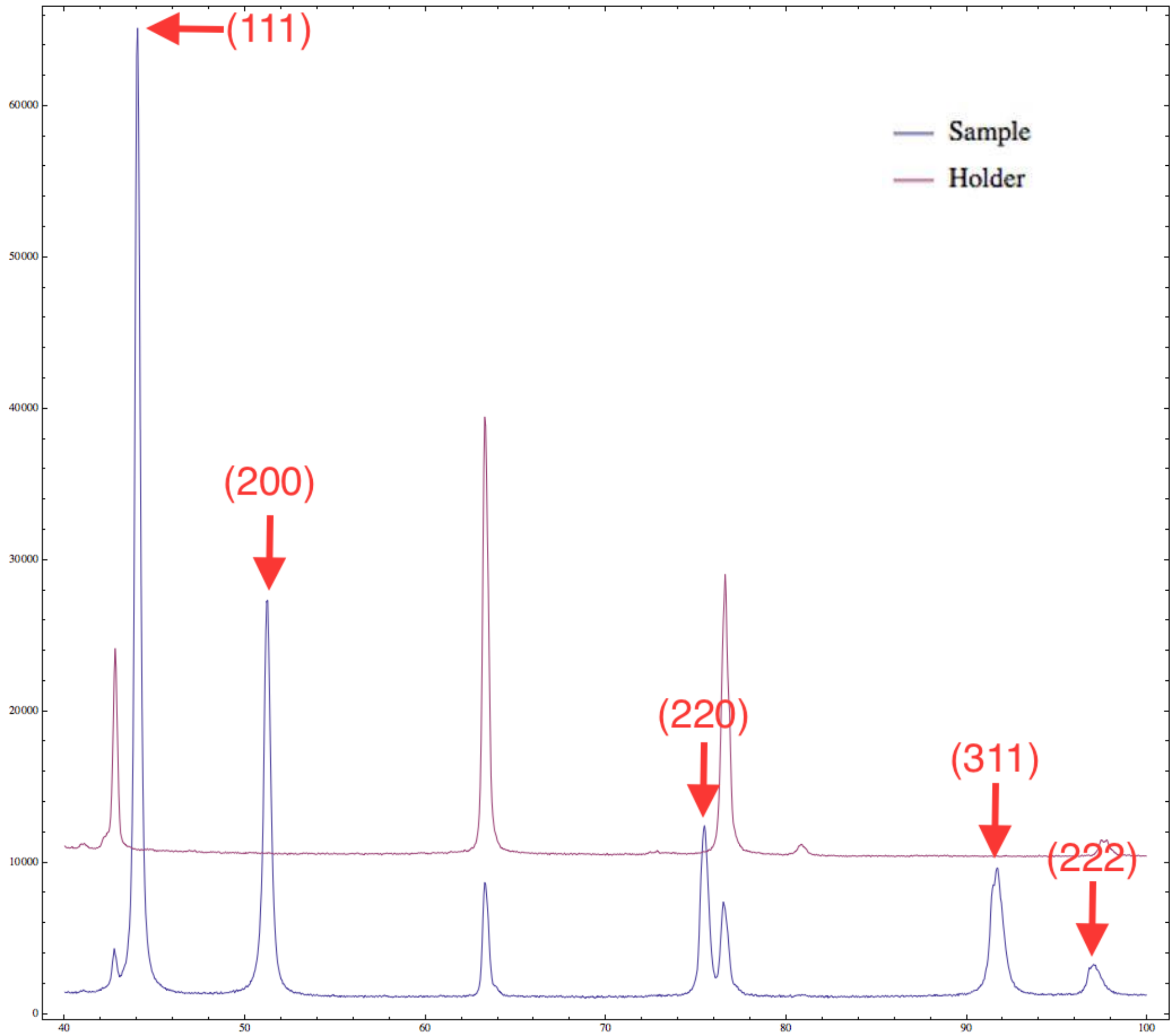

Figure 3.9 XRD plot of 2.0-unaged sample. The peaks from sample (blue) are called out with arrows. The noise peaks (red) from aluminum sample stage are shown as well.

Peak shifting is not only caused by ageing induced phase transformation but the alignment (tilt) of the specimen during the scan, can also lead to slight peak shifting. To fix shifting caused by alignment, a tiny amount of tungsten powder is uniformly placed on the surface of sample and scanned with the sample. Figure 3.10 shows the new XRD plot, which combines the plots of tungsten and Ni-Cr sample. Tungsten powder has been tested individually to calculate the reference lattice parameter. Comparing the tungsten co-scanning plot with reference tungsten plot, peak shifting from sample tilting can be calculated. The corresponding lattice parameter error from tilting can be calculated as well, which can be used to correct lattice parameters from samples.

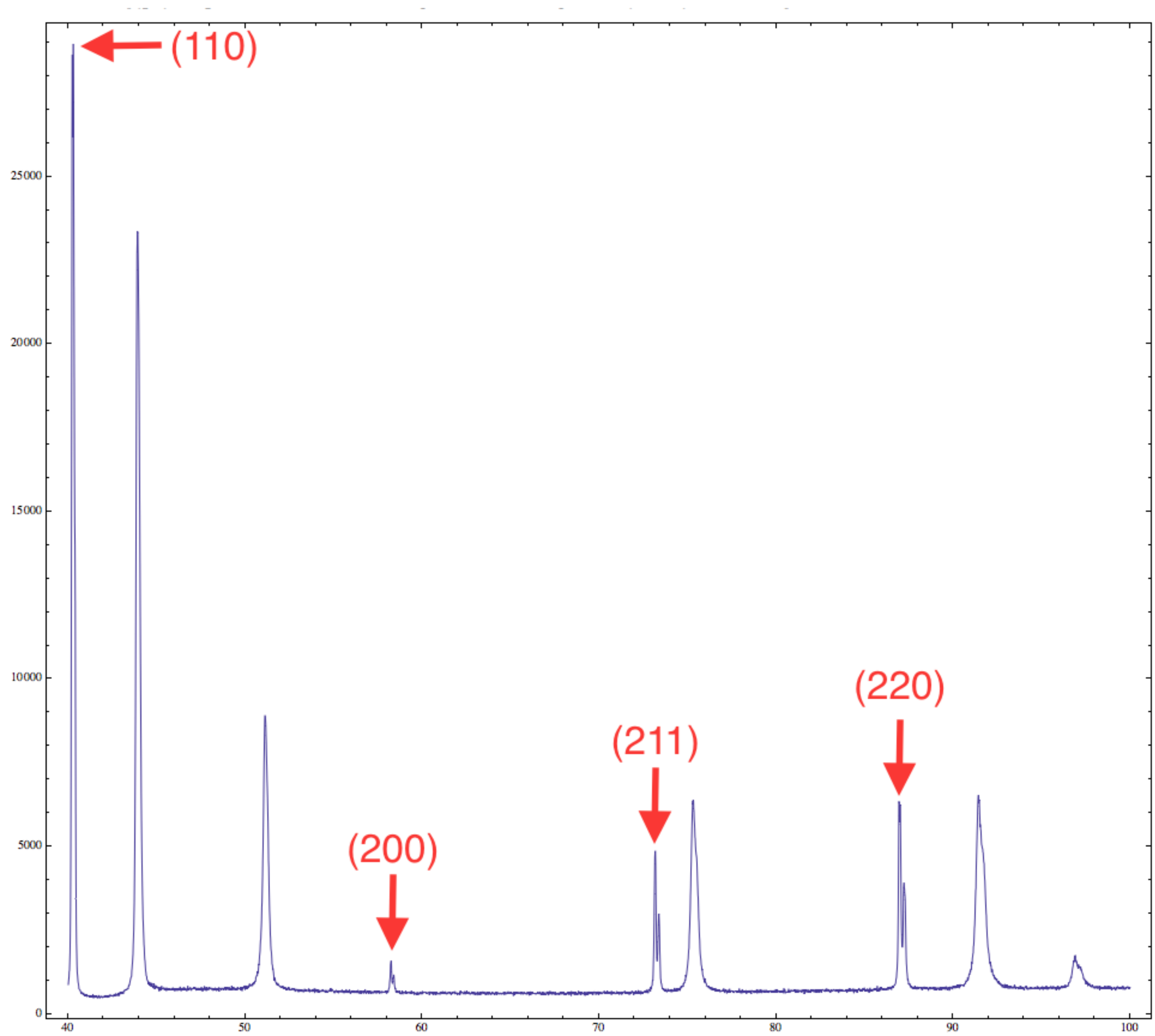

Figure 3.10 XRD plot of 2.0-unaged with tungsten powder. Tungsten reference peaks identified.

3.3.2 Precise Parameter Measurement – Cohen's Method

To perform precise lattice parameter measurements, random errors should be minimized in a reproducible and objective manner. Therefore, Cohen's Method has been used to achieve the calculation [24] using equation 2-1:

$$sin^2\theta = C\alpha + A\delta \qquad (2\text{-}1)$$

where,

$C = \lambda^2/4a_0^2$, $\alpha = (h^2 + k^2 + l^2)$, $A = D/10$, and $\delta = 10\ sin^2 2\theta$. D is a constant if a cubic substance is being examined in a Debye-Scherrer camera.

Substituting the experimental values of $sin^2\theta, \alpha$, and δ gives n equations for n reflection peaks. C and A can be solved by the method of least squares. a_0, which is defined as true lattice parameter, can be calculated directly when C is found [24].

3.3.3 System Error

As mentioned before, four reflection peaks are used to calculate four lattice parameters of a specimen. System error can be measured from the error of four reflections of four different 2.0-unaged samples after etching. Figure 3.11 shows the plot. All four samples come from one bigger piece of material with same surface condition and without any ageing. To eliminate the effect of residual stress from mechanical polishing, each sample is etched by $CuCl_2$+HCl after polishing.

Considering the influence of $K_{\alpha 2}$ wavelength causes peak separation and broadening, The EVA software program has been used to strip $K_{\alpha 2}$ effect to increase the accuracy on identifying peak angles. The calculation shows that the standard deviation of the 4 lattice parameters from 16 reflections is 0.05%, which is obviously smaller than the critical lattice contraction ~0.25% [2].

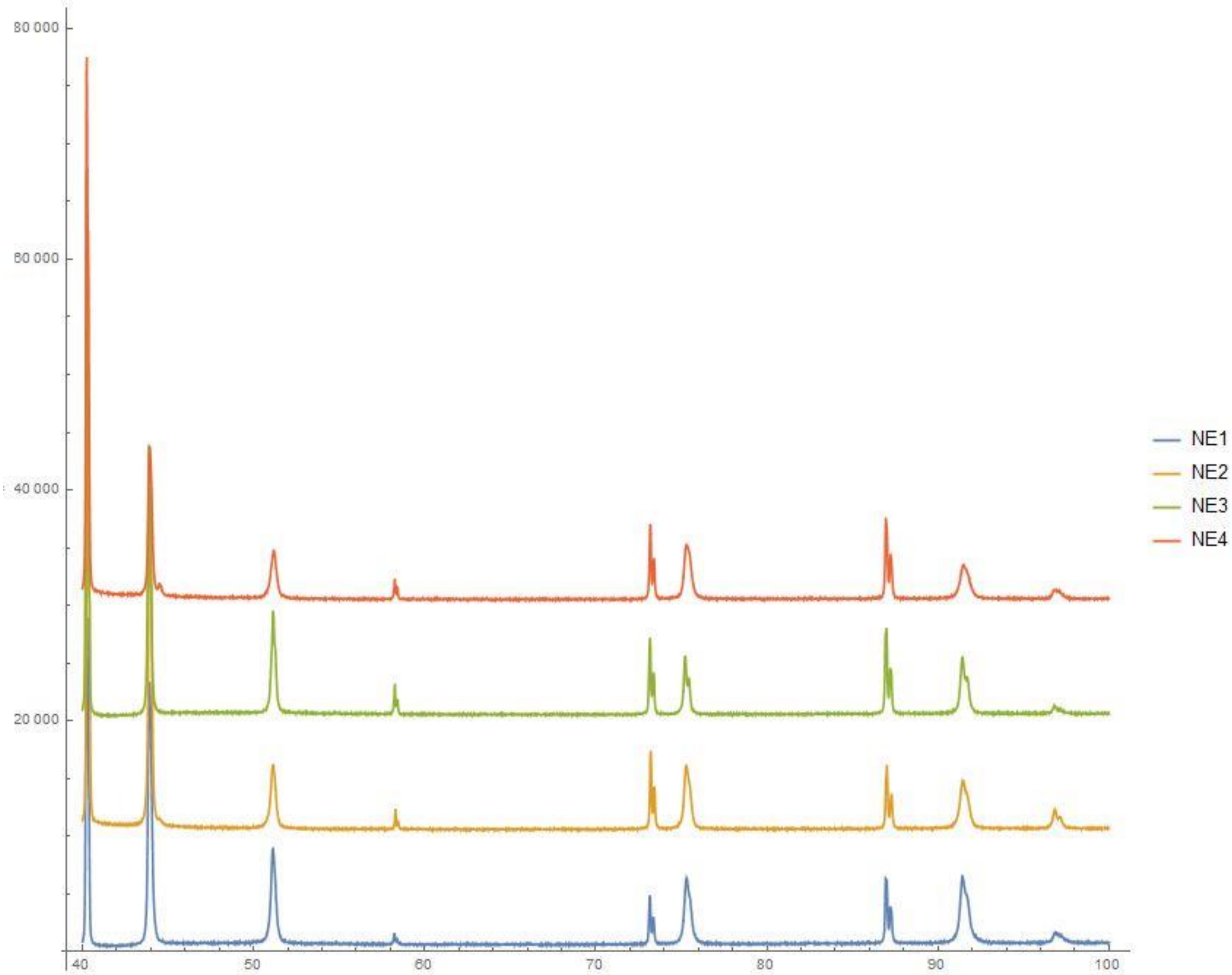

Figure 3.11 System error calculation plot (N=non-aged, E=etched).

3.3.4 Point Scanning and Area Scanning

Based on scanning area, Bruker X-ray D8, which can generate 1.5406Å wavelength, has two scanning models: point scanning and area scanning. Normal area scanning is in dimension of $10 * 25.4\, mm^2$, which will fully cover the sample. Equipped with nozzle, scanning area is reduced to a point in diameter of $1mm$. Because of the smaller area, the intensity of point scanning is lower than that of area scanning. Optical microscopy characterization of the grain size of samples reveals and average size of ~$100 - 150\mu m$. The number of grains that each scanning point will include is

$\sim 64 - 100$, which is too few to avoid occasional surface effect such as uneven polishing or etching. Therefore, area scanning is finally determined to be used in this project to perform XRD analysis.

3.3.5 Lattice Contraction for Different Stoichiometry

Lattice contraction percentage is calculated by following equation 2-4:

$$Lattice\ Contraction\ (\%) = \frac{a - a_0}{a_0} \tag{2-4}$$

Where, a_0 is the lattice parameter before ageing in unit of angstrom and it is calculated from average value of four reflections in each XRD plot. The angle of each peak is obtained by EVA program. The lattice parameter after ageing, a, is in units of Å. The lattice contraction behavior for the four stoichiometries at low (373℃), medium (418℃), and high (475℃) temperature will be discussed in the Result and Discussion chapter. One thing to note is that each lattice contraction value comes from same sample before and after ageing. All aged samples used to characterize ordering were X-rayed without etching and polishing.

3.4 Micro-hardness

Previous studies in the literature have shown that the disorder-ordered phase transformation during isothermal ageing embrittles samples, which can be correlated to a change in hardness [9]. The instrument used to perform testing is Micro Material's nanoindenter. The indenter type is Berkovich.

3.4.1 Sample Preparation

Sample preparation procedure is similar to the procedure for XRD. A flat and shinning surface is created by mechanical polishing. To avoid indentation starting on grain boundaries, each sample is etched after polishing to keep each indentation within the grains. Figure 3.12 shows the surface condition and a sample indentation.

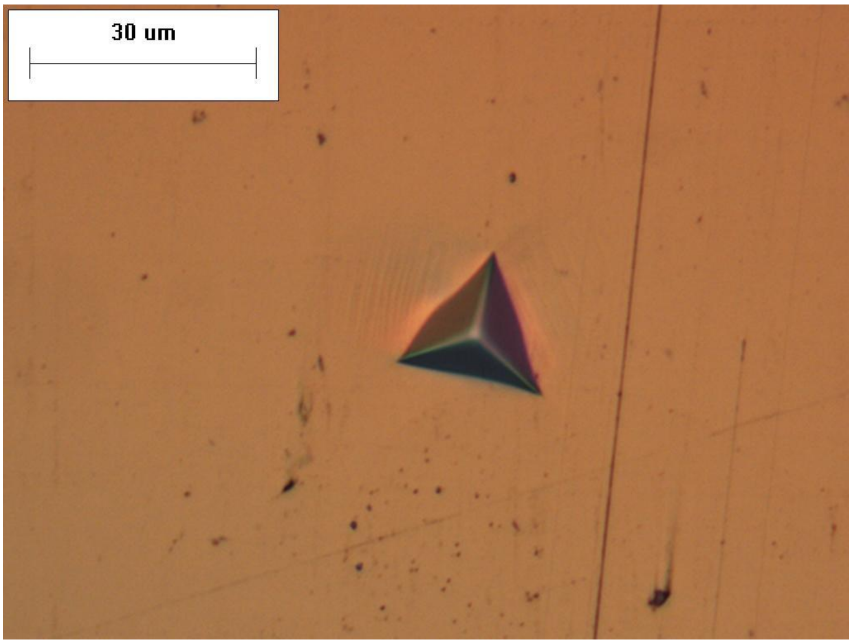

Figure 3.12 Image of indentation under optical microscope.

Figure 3.13 shows an example of depth and load plot. The load used here is 500mN and the corresponding depth is 2738 nm. The corresponding hardness is 2.95GPa.

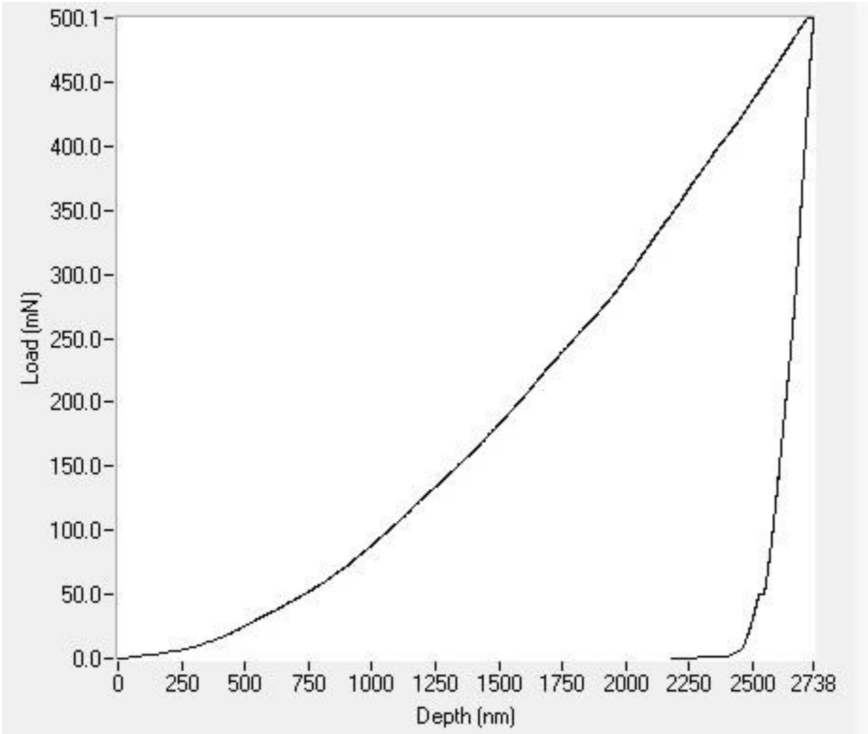

Figure 3.13 Depth and load plot (500mN).

3.4.2 Choice of Test Parameters

To perform precise and comparable hardness result, each test parameter was evaluated. Test condition includes test load (mN) and distance between indentations (μm). Sixty seconds loading time and 30s-unloading time and the dwell period for drift correction is 60s in each test. To avoid the effect of indentation on other indentation points, the distance between indentations is set to be 200μm.

3.4.3 Test Load

Test load will influence the surface condition and sensitivity of micro-hardness test. Too large of a test load may destroy the shape of indentation or even crack sample. Both may affect the test results. Too small of a test load will increase the sensitivity of each test, which will increase the probability of being disturbed by environmental vibration of surface inhomogeneities.

To determine an appropriate test load, ten indentations with different loads, which are from $500mN$ to $5N$ in a step of $500mN$, are tested. Each load test was repeated 10 times. The depth vs load plot is shown in Figure 3.14. Figure 3.15 shows the indentation under 5 and $4.5N$. Figure 3.14 also shows that the standard deviation for 10 indentations is $0.176GPa$. Considering the potential risk of non-uniform edges to test result and the higher convergence in low load, the $500mN$ load is selected to perform hardness testing. This load is also consistent with previous micro-hardness studies in the literature [18].

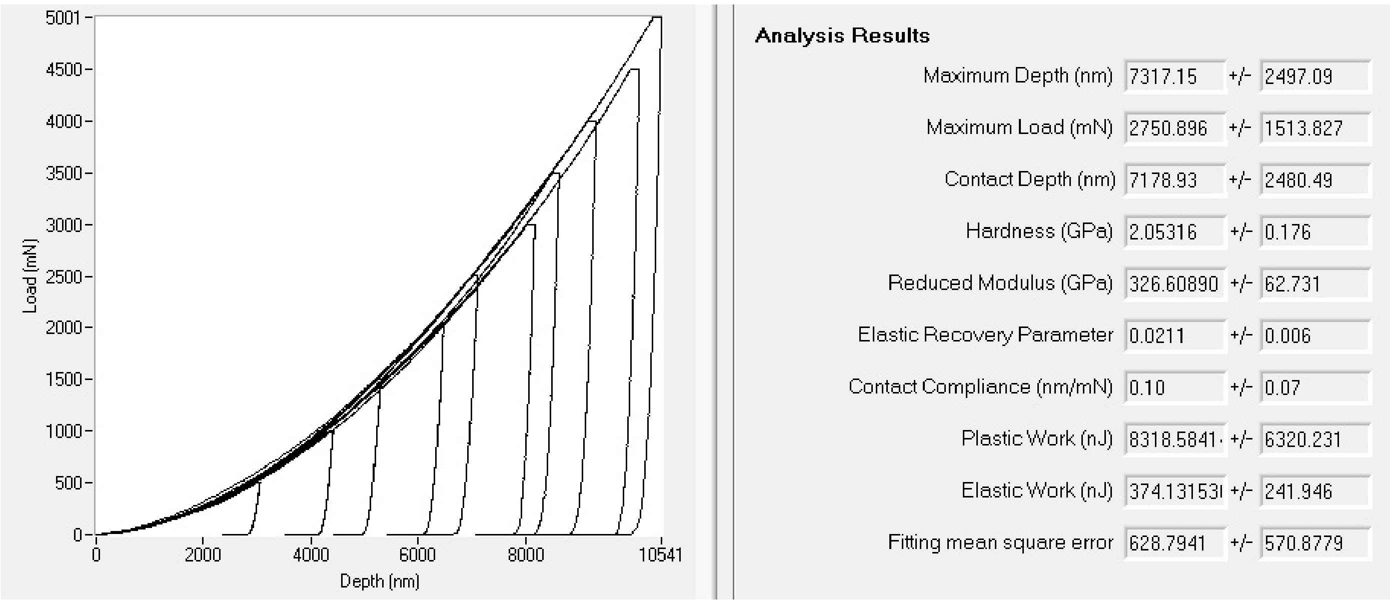

Figure 3.14 Depth vs load plot and corresponding analysis result (vary loads).

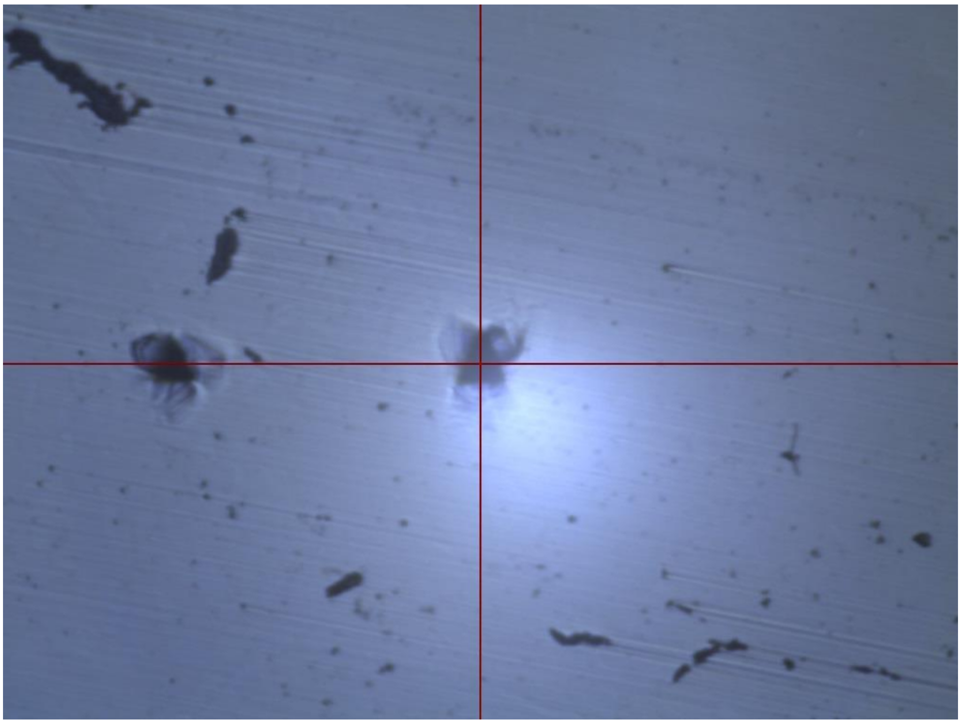

Figure 3.15 Image of indentation under 4500 mN (left) and 5000 mN (right).

3.5 Transmission Electron Microscopy (TEM)

Compared to the previous two techniques, TEM is the most straightforward method to confirm the formation of LRO phase. The characterization procedure includes sample preparation and TEM diffraction pattern inspection.

3.5.1 Sample Preparation for TEM

All samples for TEM in this project were made by the focused ion beam (FIB) lift out method. A Quanta 3D SEM was used for FIB lift out and a Quanta Helios for thinning and polishing. Samples were polished in optical characterization quality first, then samples were send to coating machine to coat 10nm carbon layer and 30nm chromium layer. The reason of coating is to prevent beam damage and ion implantation during later thinning in Quanta Helios SEM. Beam damage and impurity ion implantation will destroy the ordered phase, which will affect the TEM analysis.

After loading the sample in Quanta 3D SEM, a $0.50\mu m$ platinum protection layer will be coated on sample surface (Figure 3.16). The goal of coating protection layers is also to minimize beam damage or gallium ion implantation during cutting, which allows for higher cutting voltage and current to decrease sample preparation time.

After coating, the specimen will be lifted out (Figure 3.17) and welded on a copper grid in the Quanta 3D (Figure 3.18), then the sample will be transferred to Quanta Helios for more thinning to decrease the thickness less than $100nm$ (Figure 3.19 to Figure 3.21), because the maximum thickness for electron passing through nickel is 98nm [25]. After thinning, samples need to be polished under 2MeV and 500keV to minimize the effect of gallium implantation.

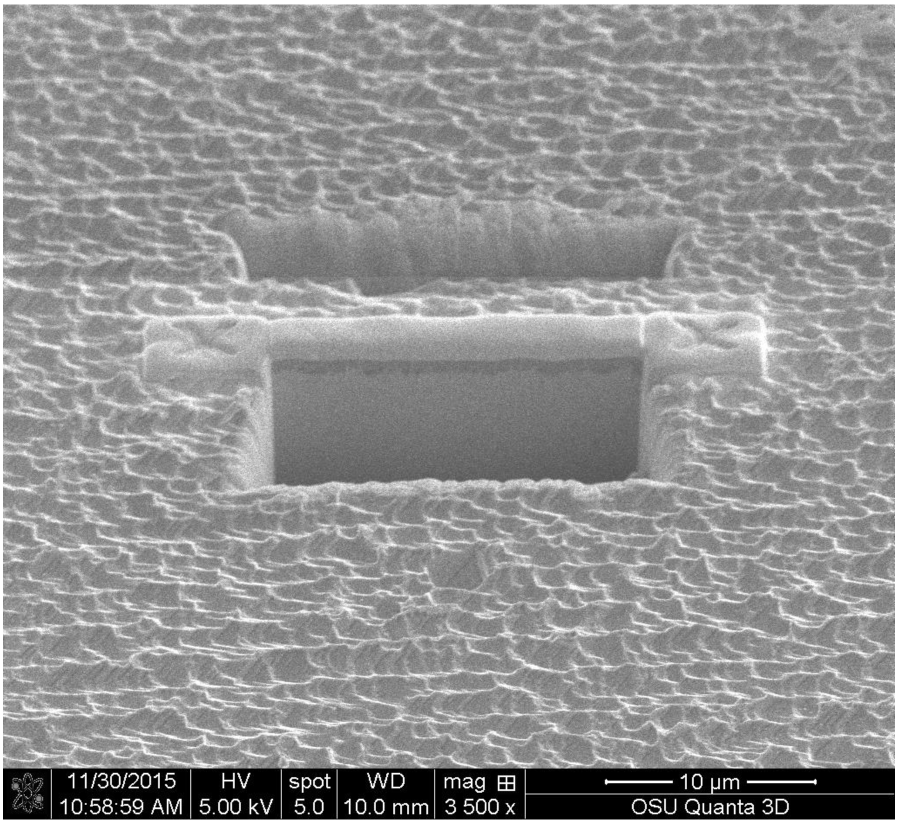

Figure 3.16 FIB protection layer and cross-section.

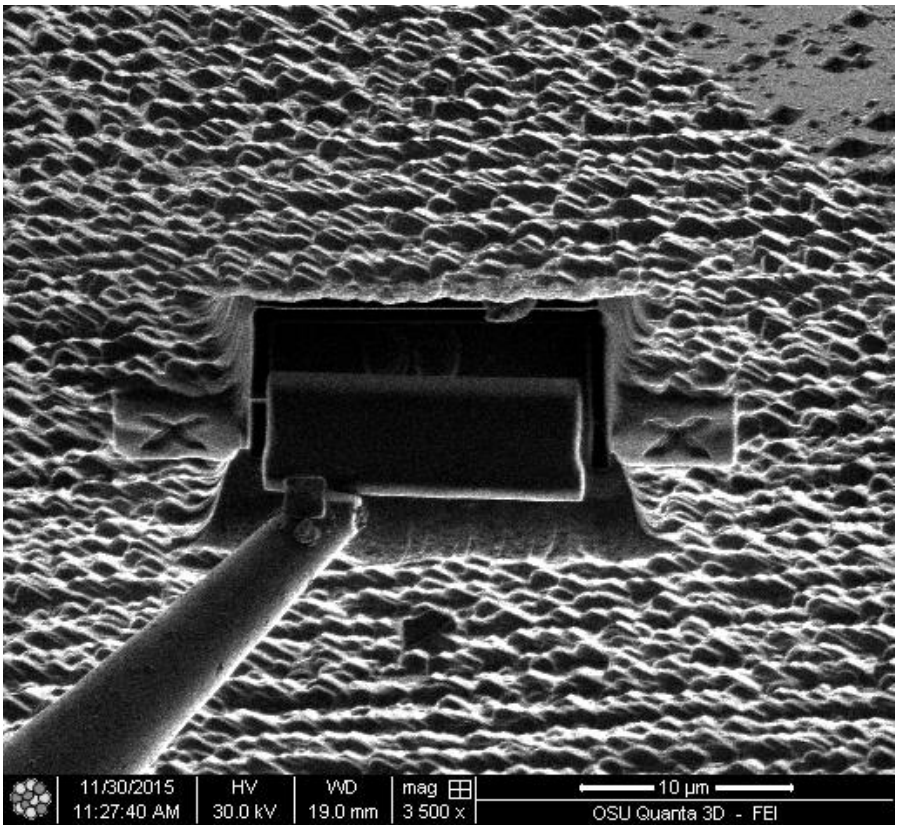

Figure 3.17 Specimen Lift-out.

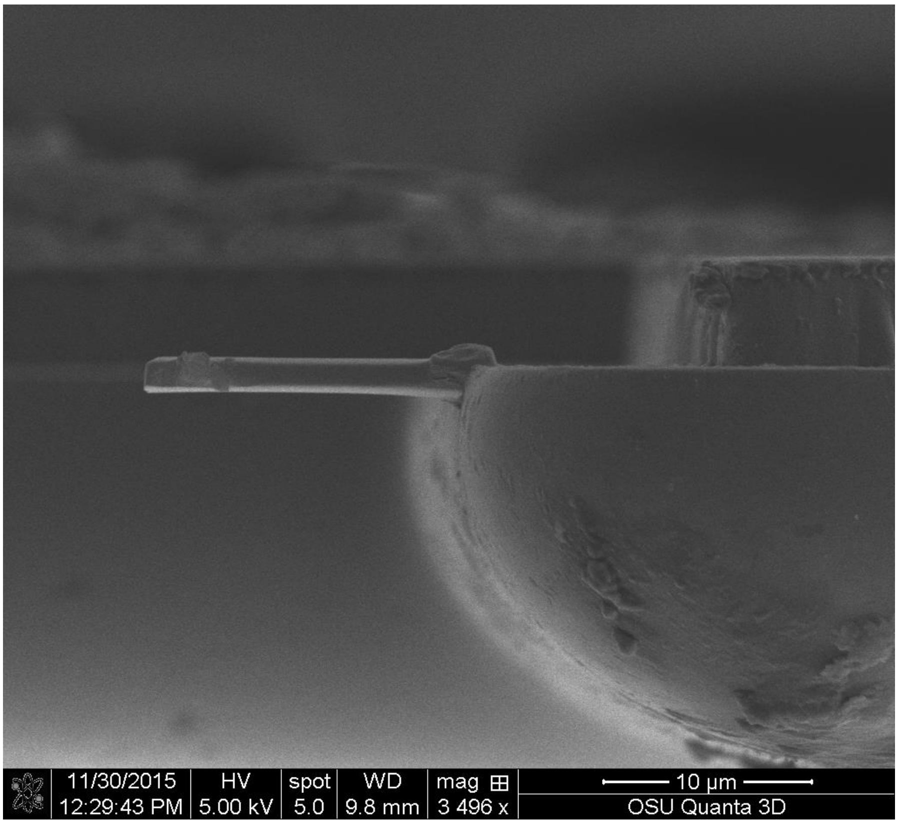

Figure 3.18 Specimen welded on a copper grid.

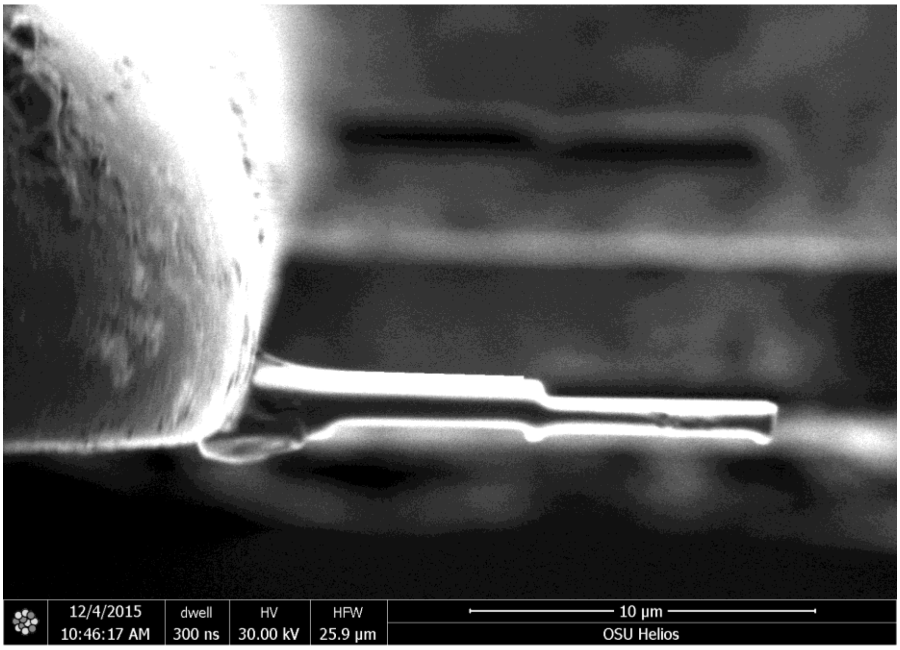

Figure 3.19 Thinning in progress.

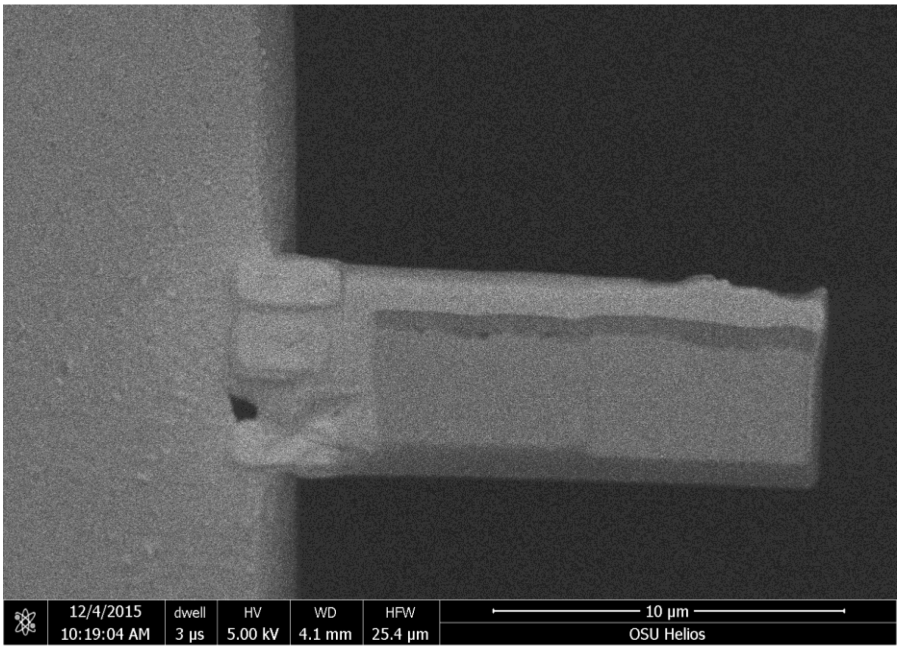

Figure 3.20 Specimen before thinning.

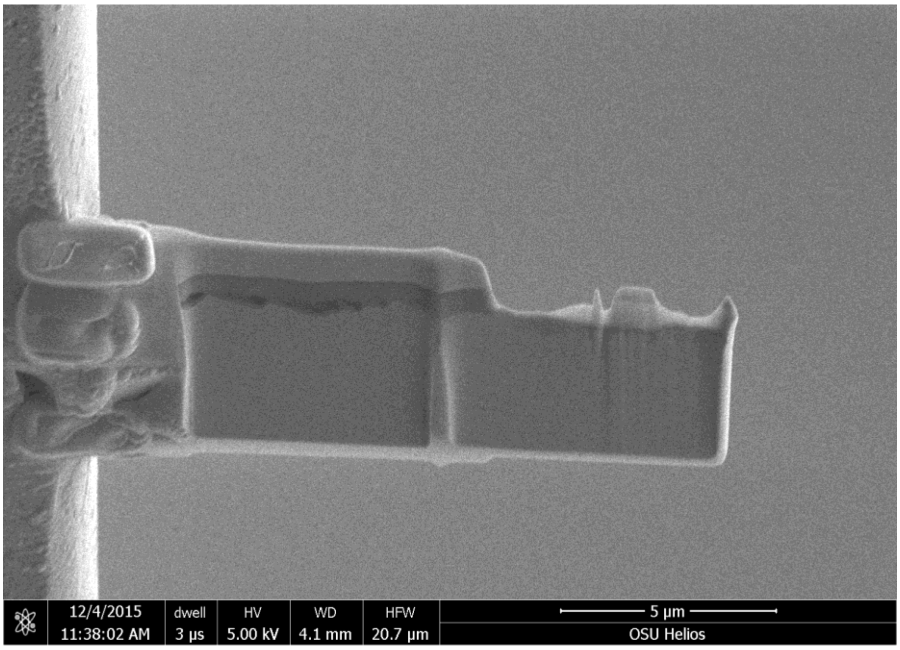

Figure 3.21 Specimen after thinning

3.5.2 TEM Inspection

Considering the structure of the LRO phase, superlattice reflection in the diffraction pattern can be seen in every zone axis. Figure 3.22 shows an example of diffraction pattern from similar materials, which are a Ni-Cr-3Fe ternary alloy (top left, top right, and bottom right) and $Ni_2(Cr_{0.5}Mo_{0.5})$ alloy (bottom left) [5, 21]. This means the formation of LRO phase can be confirmed if secondary reflection can be identified in any zone axis.

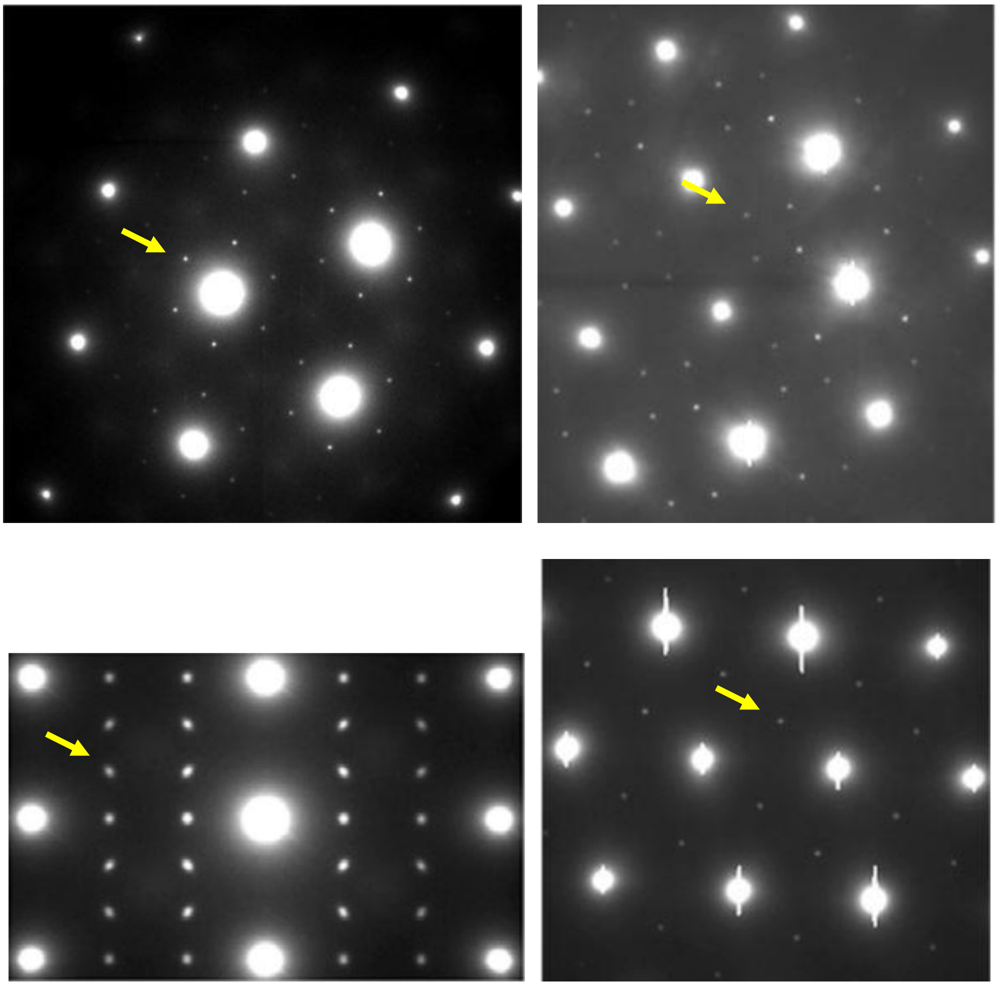

Figure 3.22 TEM diffraction pattern of ordered phase in different zone axis of similar materials (top left: [111], top right [001], bottom left [112], bottom right [011]) [5, 21].

4 Chapter 4 - Result and Discussion

4.1 Isothermal Heat Treatment Record

Stoichiometric samples underwent isothermal heat treatments at temperatures of 373°C, 418°C, and 475°C. Figure 4.1 gives a part of temperature record, which is from 2/16/2015 12:00 pm to 3/30/2015 2:33 pm, as an example. The standard deviation of each temperature are 0.076°C (for 373°C), 0.045°C (for 418°C), and 0.058°C (for 475°C).

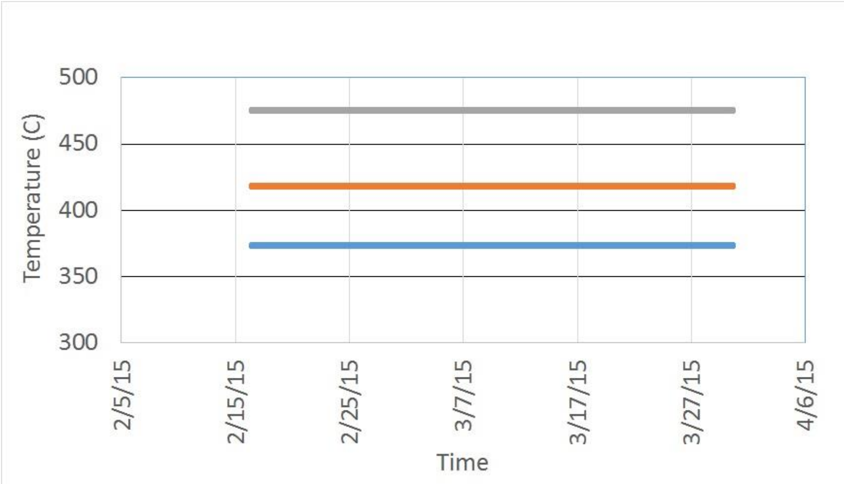

Figure 4.1 Sample of temperature record of heat treatment.

4.2 Result of X-ray Diffraction

Based on previous tests and calculation on lattice parameter, lattice contractions for different stoichiometry are calculated by comparing lattice parameter of each sample before and after ageing. Effect of mechanical polishing, following residual stress on lattice parameter, and disturbing of surface oxide caused by heat treatment are shown in this section as well.

4.2.1 Lattice Contraction for Different Stoichiometry

Figure 4.2 to 4.4 shows the lattice contraction results as a function of temperature. The result shows that: 1) At the lowest temperature, most lattice contractions are evident after 1000 hours. However, the sample with $\frac{Ni}{Cr} = 2.2$ composition shows no lattice contraction after 5000 hours. 2) At the medium temperature (418°C), the lattice contractions for most alloys become evident around 500 hours ageing, which is faster than at 373°C, but the relationship between stoichiometry and rate of ordering is difficult to determine. Some samples have lattice contraction followed by lattice expansion, probably due to the release of residual stresses during the heat treatment (Figure 4.3). The standard deviation of medium temperature is much larger than that of low and high temperature, which makes analysis more difficult. 3) At the highest ageing temperature (475℃), the lattice contraction behavior is more obvious than at lower temperatures (Figure 4.4). The reason is that the ordering transformation is controlled by both nucleation and diffusion. All ageing temperatures are lower than critical value, which is about 525℃ [2] but the peak transformation rate is near 475°C [5]. Results show that the 1.8 composition has the fastest ordering rate, which is conflicting with previous research result that stoichiometric alloys have a faster ordering rate than off-stoichiometric alloys [4]. It needs to be noticed that maximum lattice contractions are ~ 0.4 to 0.6%, which is much higher than the critical value (~0.25%) from previous papers. The large lattice contraction is potentially caused by three reasons: releasing of surface residual stress that comes from polishing, calculation method of lattice parameter, and absence of high angle peak in calculation.

Compare with the experiment from Young, there are two different points in XRD and corresponding sample preparation [ref]. First, Young polished samples via electropolishing, which can remove surface oxide without remaining residual stress. In this thesis, mechanical polishing has been used to perform flat and clean surface. Second, both Young and Marucco used only one reflection around 140° to calculate lattice parameter instead of the average value of several peaks in this thesis to calculate lattice contraction.

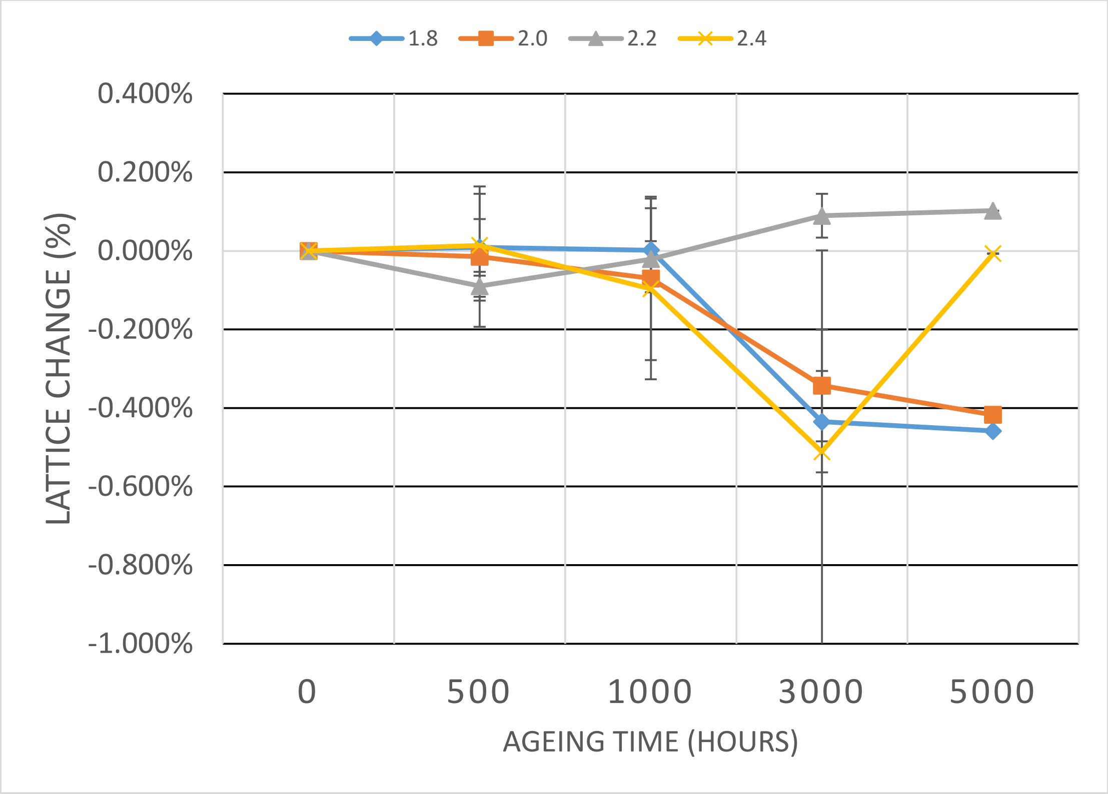

Figure 4.2 Lattice contraction at 373℃ up to 5000 hours.

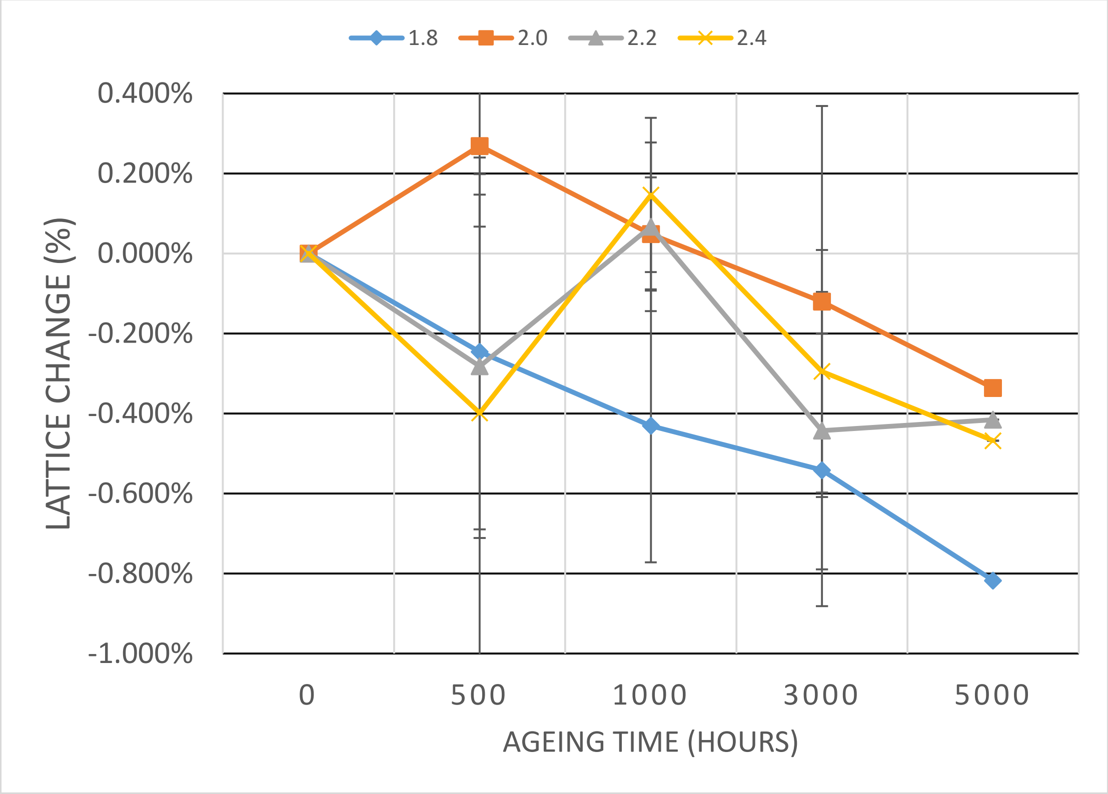

Figure 4.3 Lattice contraction at 418℃ up to 5000 hours.

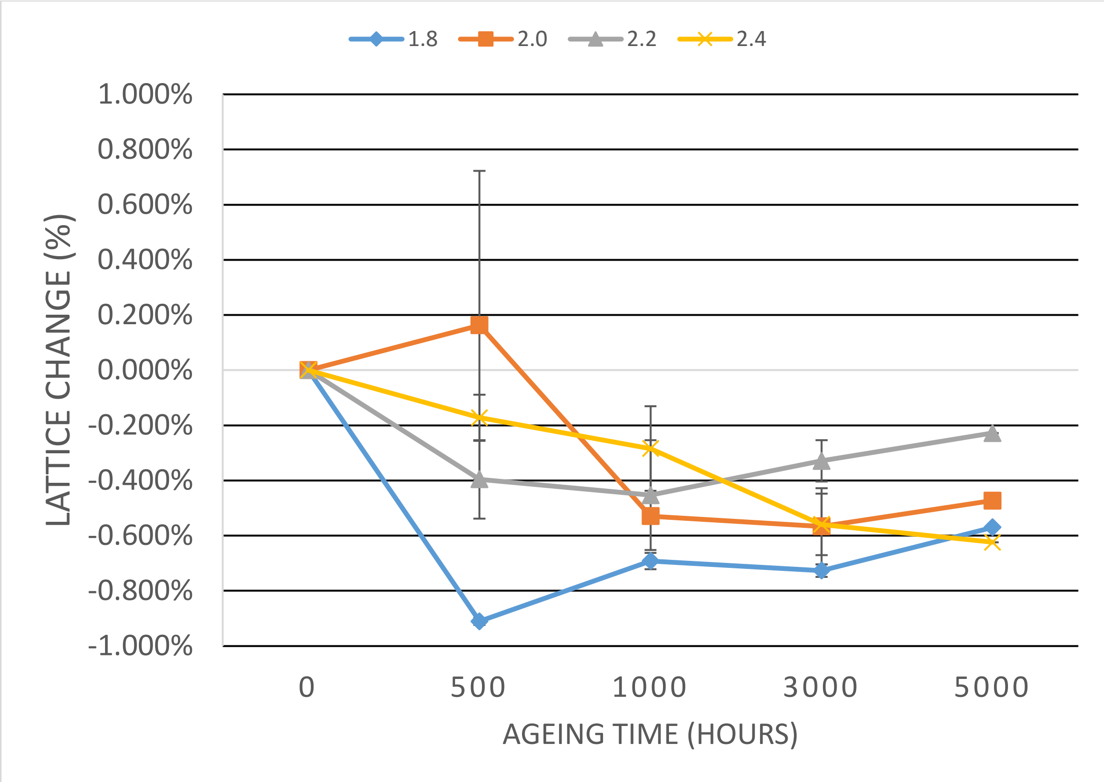

Figure 4.4 Lattice contraction at 475℃ up to 5000 hours.

4.2.2 Effect of Mechanical Polishing on Lattice Parameter Measurement

Figure 4.5 shows the comparison of XRD plot between un-etched (with residual stress from polishing) and etched (without residual stress) sample after mechanical polishing.

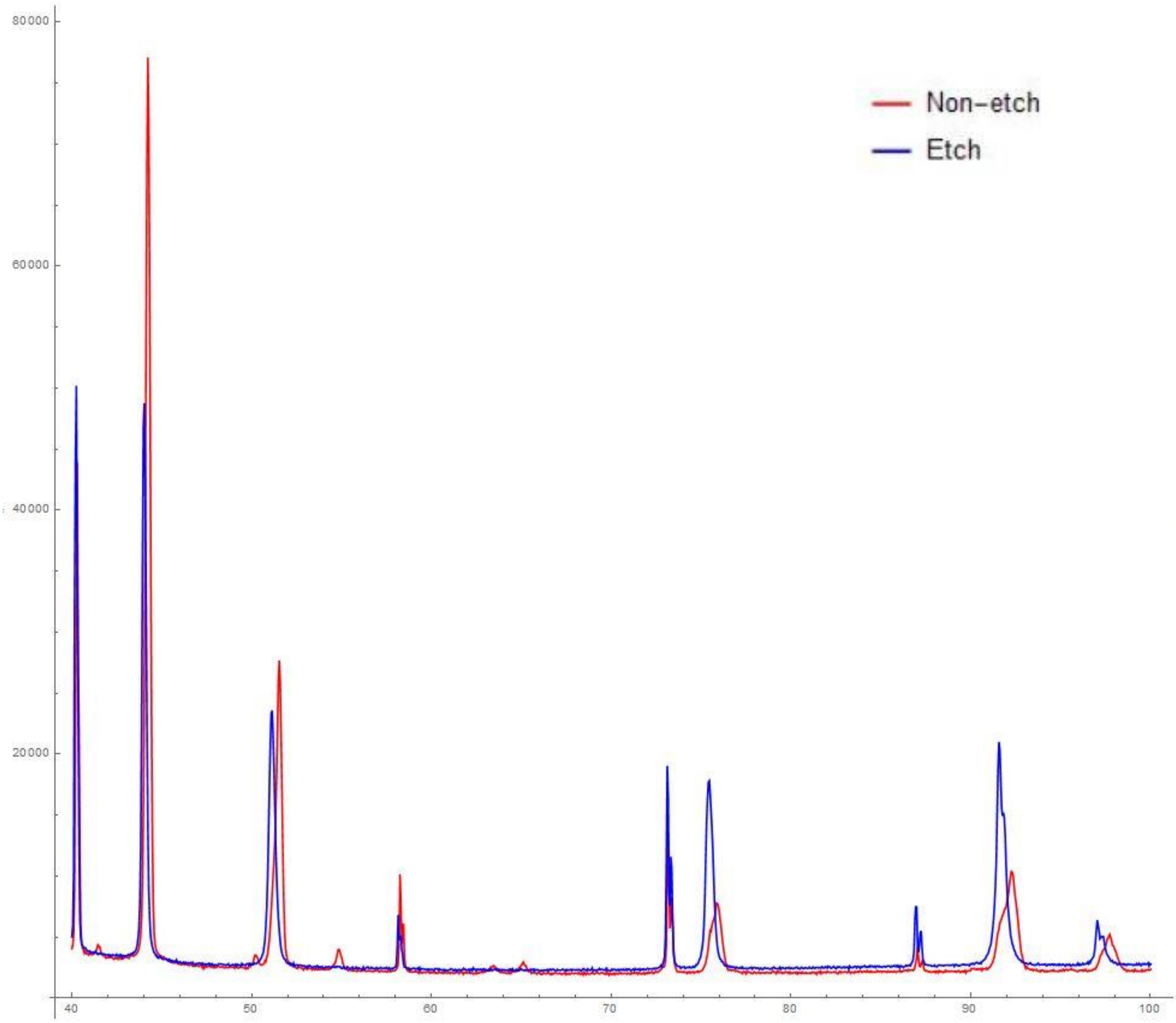

Figure 4.5 Un-etched (with residual stress) vs etched (removed residual stress) sample (sample ID: 2.0-3000 hours @475 ℃)

After calculating by Cohen's Method, the lattice parameter before etching is 3.54182Å and it changes to 3.56230Å after etching. The result shows that mechanical polishing can decrease the lattice parameter, which can be observed as peak shifting in Figure 4.5. Same phenomenon can be observed in unaged samples as well. There are two reasons: the energy of X-day and residual stress that come from polishing. The wavelength of x-ray from Bruker D8 is 1.5406Å. Calculation results show that the X-ray depth is shallow corresponding to the layer that is still influenced by residual stress. The proof is that lattice parameter of un-etched sample is smaller than that of etched sample.

However, etching is not the solution to release residual stress and lattice parameter measurement. Table 4.1 shows the lattice contraction result after etching. All lattice parameters come from the same samples. The only difference is the surface condition. The samples used to clarify the effect of etching come from $\frac{Ni}{Cr} = 2.0$ aged at the high temperature 475℃. Result shows that after etching, all samples show lattice expansion towards a similar value (~0.07%) instead of contraction. All lattice parameters will rise up to a similar value (~3.56Å) as well.

Table 4.1 Lattice parameter after etching (sample: 2.0 aged at 475℃), a is lattice parameter after etching, a_0 is lattice parameter before etching. All samples have been aged.

Aged Time (hours)	a_0 (Å)	a (Å)	Δa (Å)	Change %
500	3.55890	3.56158	+0.00268	+0.0753
1000	3.56167	3.56488	+0.00321	+0.0901
3000	3.56588	3.56800	+0.00212	+0.0595

4.2.3 Effect of Oxide

Figure 4.6 shows the difference on surface condition before and after isothermal ageing. A black oxide layer on the sample surface can be observed by the naked eye. XRD reflection (Figure 4.7) shows that the oxide leads to peak broadening in addition to peak shifting. Unpolished sample (left) is the initial condition after ageing in furnace. Polished sample (right) is polished in optical characterization quality without etching.

Figure 4.6 Sample surface after (left) vs before (right) ageing.

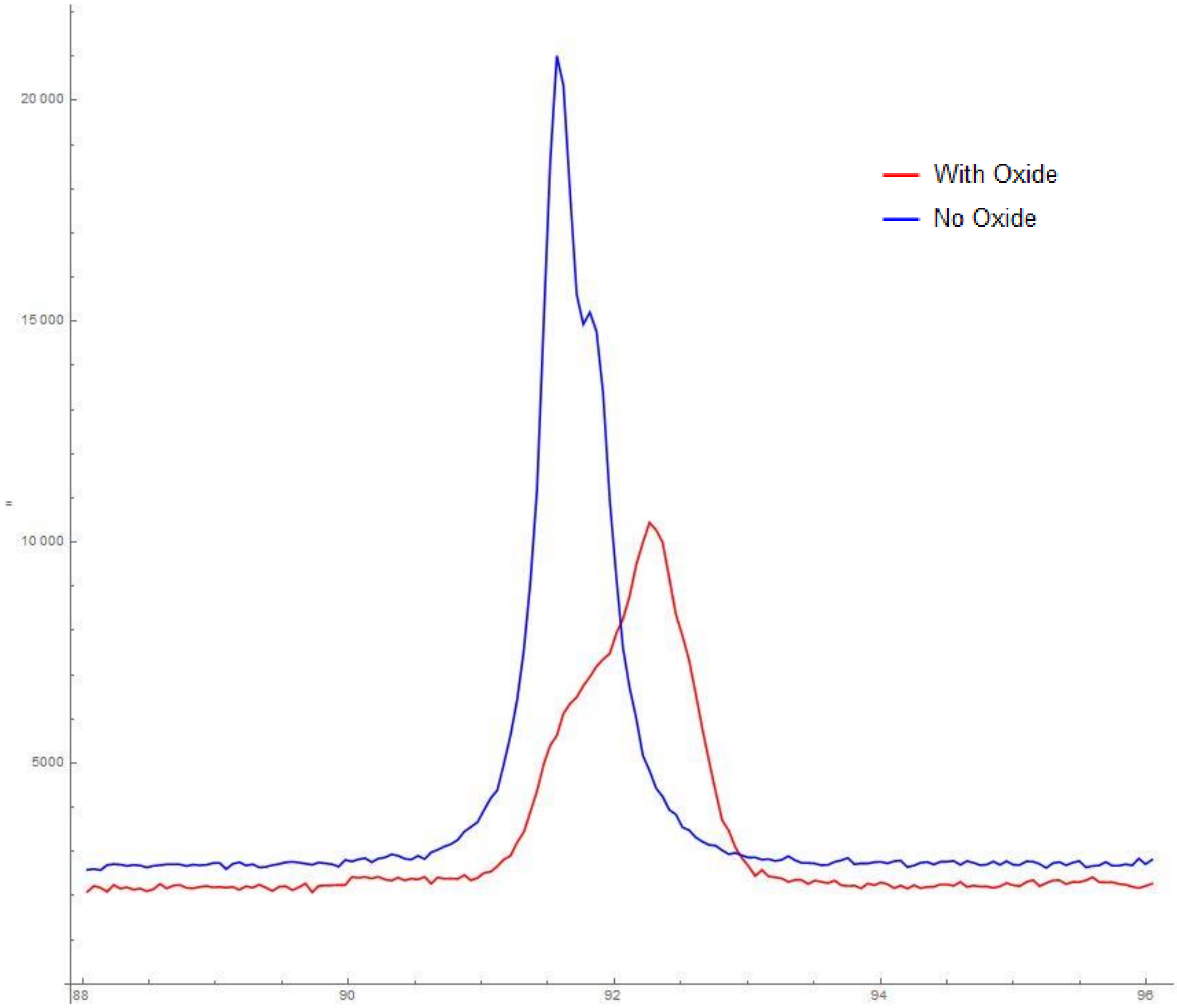

Figure 4.7 XRD reflections (311) with (no polishing) vs without oxide (polished and etched) (sample 2.0-3000 hours@475℃).

Reflections show that the oxide on surface causes peak (311) broadening and separation, which increases with ageing. The red curve has normal peak separation caused by $K_{\alpha 1}$ and $K_{\alpha 2}$ wavelength. The blue plot shows a wider peak and peak separation by forming a new structure. The new peak is on left side of the old reflection peak. This makes precise angle identification more difficult. By fitting reflections with database, the structure of oxide is closed to Ni_2O_3H (Figure 4.8). Another two potential reasons that may cause peak boarding are increasing of grain size and instrument effects [26]. Since the comparison comes from one specimen before/after polishing, these two reasons cannot be the primary reason that cause boarding.

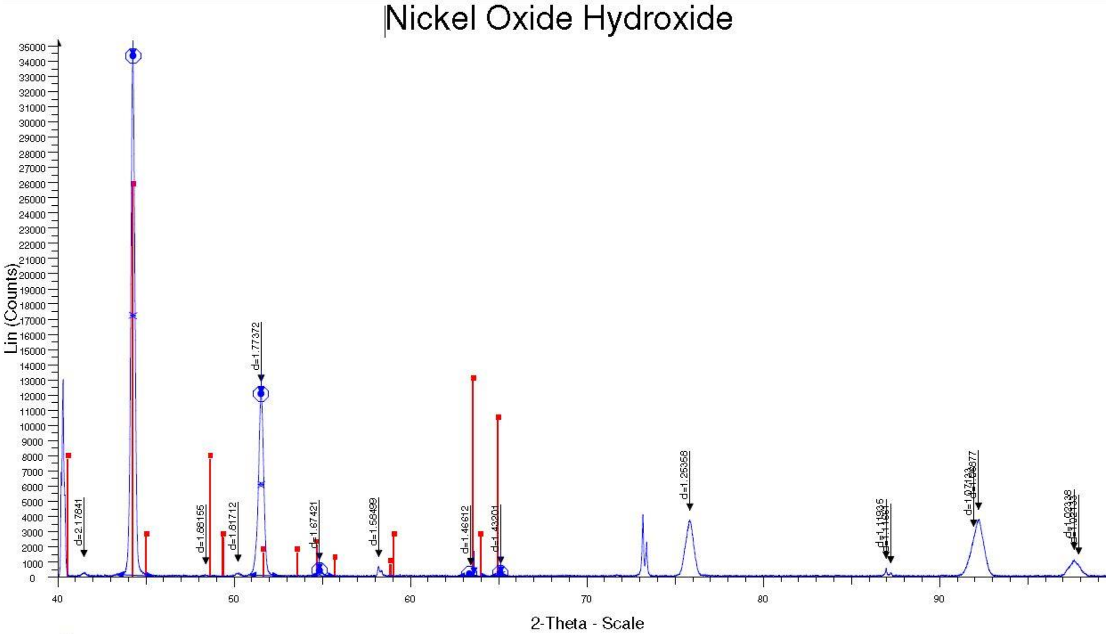

Figure 4.8 Fitting oxide structure with database.

Considering uncertainty on calculation both sensitivity on surface condition, XRD would not be the best method to identify the relationship between ordering rate and stoichiometry.

4.3 Result of Micro-hardness

4.3.1 Hardness Result

Hardness comparisons between different compositions, ageing times and temperatures will be reported in this section. For each sample, twenty indentations are randomly preformed with 500mN load and a Berkovich indenter. The corresponding standard deviation distributes from 2.34 to 11.69%, which means the largest standard deviation is still much smaller than measured values.

Figure 4.9, Figure 4.10, and Figure 4.11 show the hardness result for all specimens after ageing at low 373℃, medium 418℃, and high temperature 475℃ for ageing times up to 5000 hours. Figure 4.12 shows relationship between ordering rate and stoichiometry at low, medium, and high temperatures.

At low temperature (373 ℃), Figure 4.9 shows that stoichiometric samples have faster ordering rate than off-stoichiometric samples. Among off-stoichiometric samples, 2.4 samples, which are lowest in chromium, have the lowest ordering rate. Another phenomenon need to be noticed is that the 2.0 and 1.8 samples show a hardness decrease after initial hardening and similar softening happens for the 2.2 sample after ageing for 5000 hours. Figure 4.12 shows this behavior as well. The potential reason for their unstable ordering behavior is that the increasing on micro-hardness is still small and it will be easier influences by system error compared to the large increasing on micro-hardness at high temperature. The unstable embrittlement behavior shows that samples are not fully ordered at 373℃ after heat treatment for 5000 hours.

At 418℃, the ordering behavior is similar for all compositions. Different degrees of softening can be observed at all compositions. Due to the higher ageing temperature and higher diffusivity of Cr, rate of hardening (ordering) is faster in Cr-rich sample than that at low temperature.

Finally, when the ageing temperature rises to 475℃, the stoichiometric samples have a higher ordering rate than off-stoichiometric samples, which is same at low temperature 373℃ but difference is more obvious at high temperature. For off-stoichiometric samples, the behavior is similar to low temperature, which means stoichiometric samples are of faster ordering rate than off-stoichiometric ones.

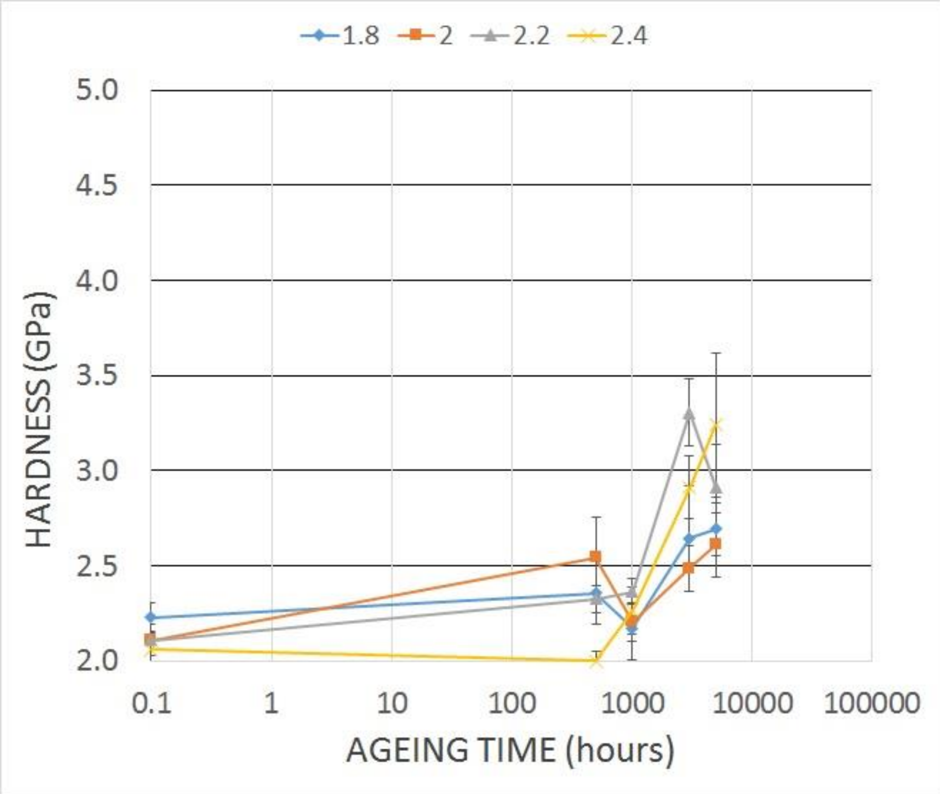

Figure 4.9 Hardness data at 373℃ up to 5000 hours.

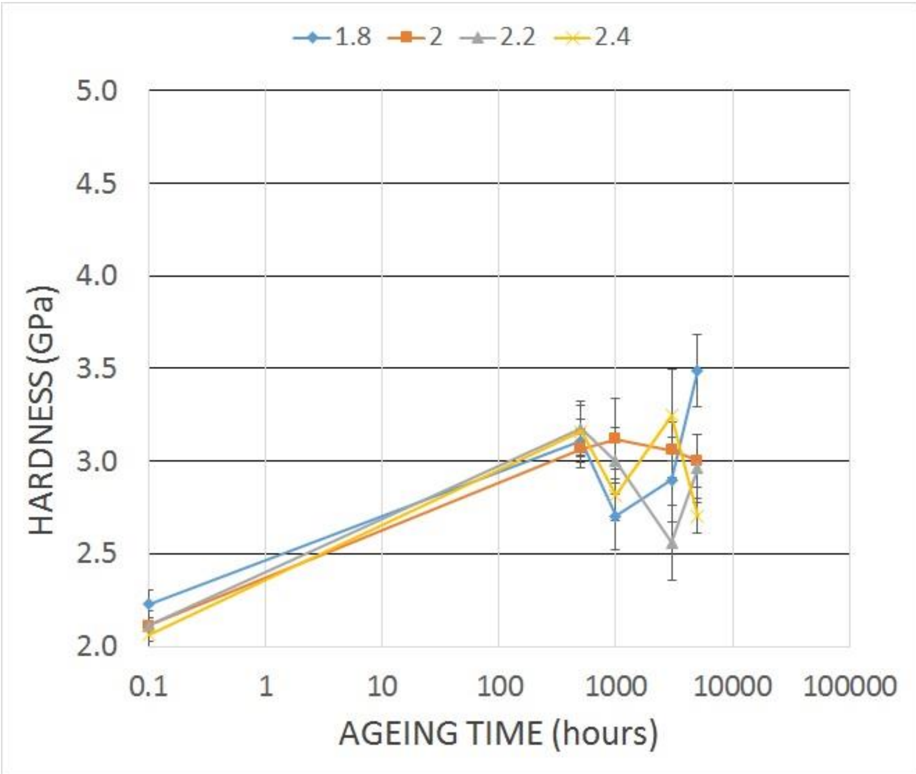

Figure 4.10 Hardness data at 418℃ up to 5000 hours.

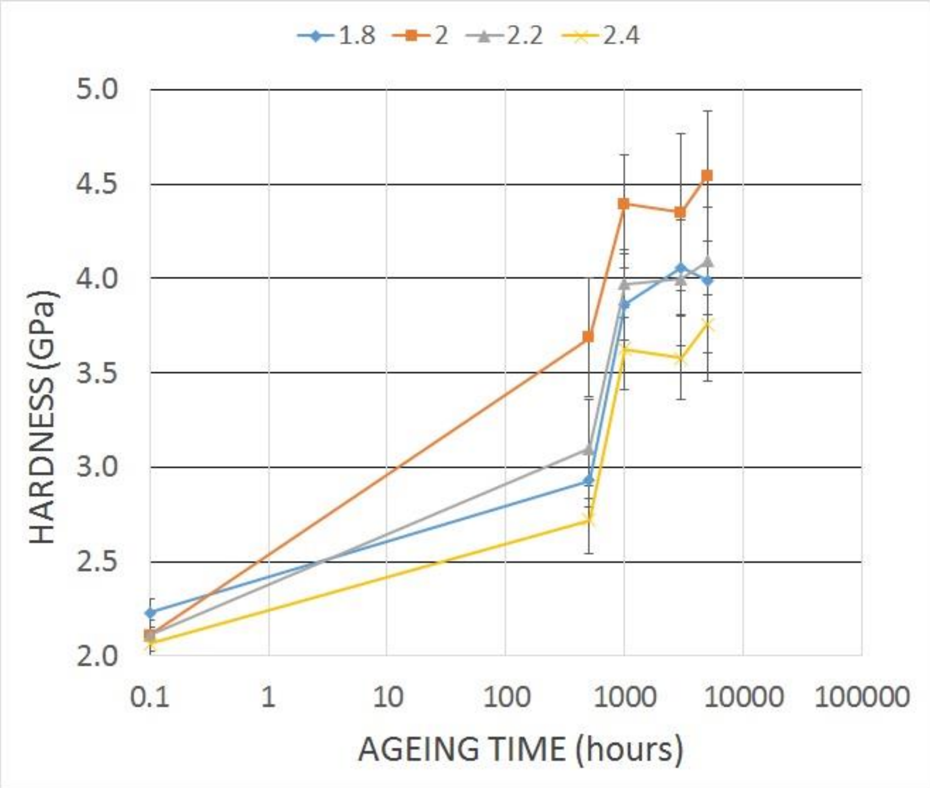

Figure 4.11 Hardness data at 475℃ up to 5000 hours.

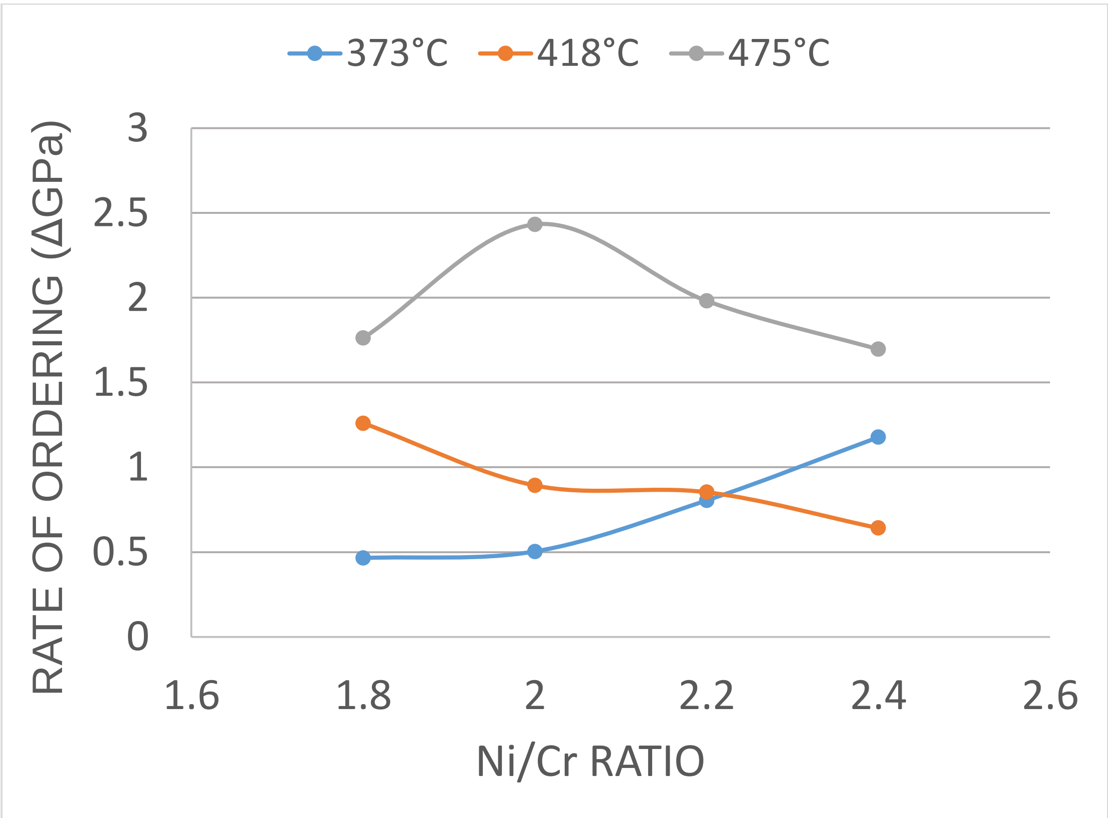

Figure 4.12 Relationship between ordering rate and stoichiometry at low, medium, and high temperatures after 5000 hours ageing.

4.3.2 Comparison between XRD and Micro-hardness

The corresponding standard deviation distributes from 2.34 to 11.69% for micro-hardness result, which means the largest standard deviation is still much smaller than measured values. The results have been shown in last section from Figure 4.9 to Figure 4.11. Compared to the small error of micro-hardness result, the error of lattice contraction from XRD is larger and unpredictable. The only result that can be concluded from XRD is higher ageing temperature enhances ordering transformation. The role of stoichiometry in ordering is disturbed by other effect such as polishing, etching, and surface oxide.

4.4 Result of Transmission Electron Microscopy (TEM)

Figure 4.13 shows diffraction patterns from 2.0 stoichiometry samples, which are aged at 373℃ for 3000 hours (left in Figure 4.13) and aged at 418℃ for 3000 hours (right in Figure 4.13), with no ordered phase. Without a significant amount of LRO superlattice structure, no secondary diffraction is identified in the diffraction patterns.

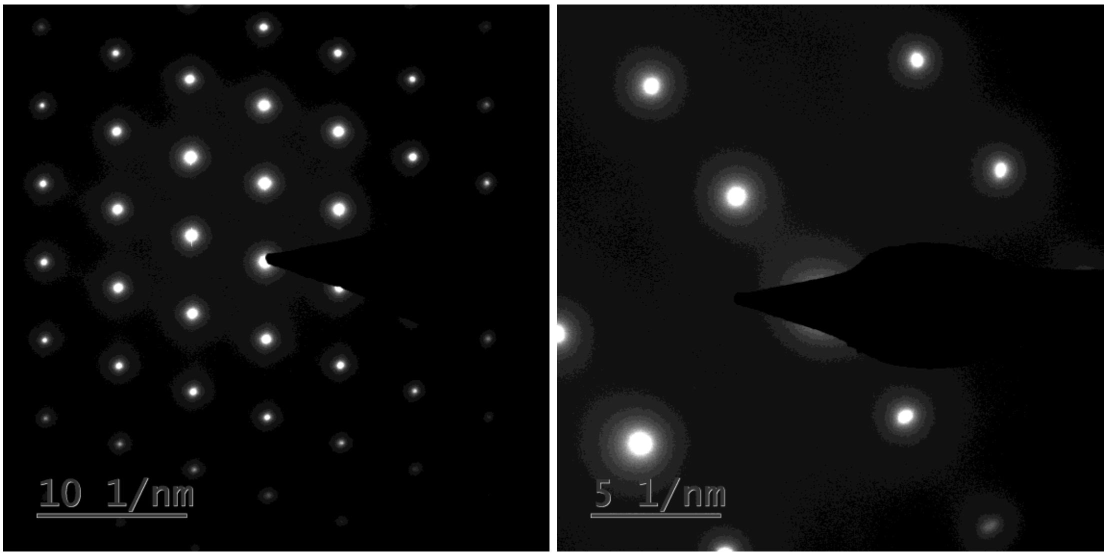

Figure 4.13 Diffraction pattern in 2.0 @373 ℃-3000hrs (left) and 2.0 @418 ℃-3000hrs (right).

Figure 4.14 shows diffraction patterns from some samples in four zone axis, which give superlattice reflections (top left and top right: 2.0 sample at 475℃-3000hrs, bottom left and bottom right: 2.0 sample at 475℃-5000hrs). Table 4.2 shows the confirmation result of $\frac{Ni}{Cr} = 2.0$ samples at different ageing time. To avoid unnecessary test, the result of micro-hardness is considered to be the guideline of TEM characterization.

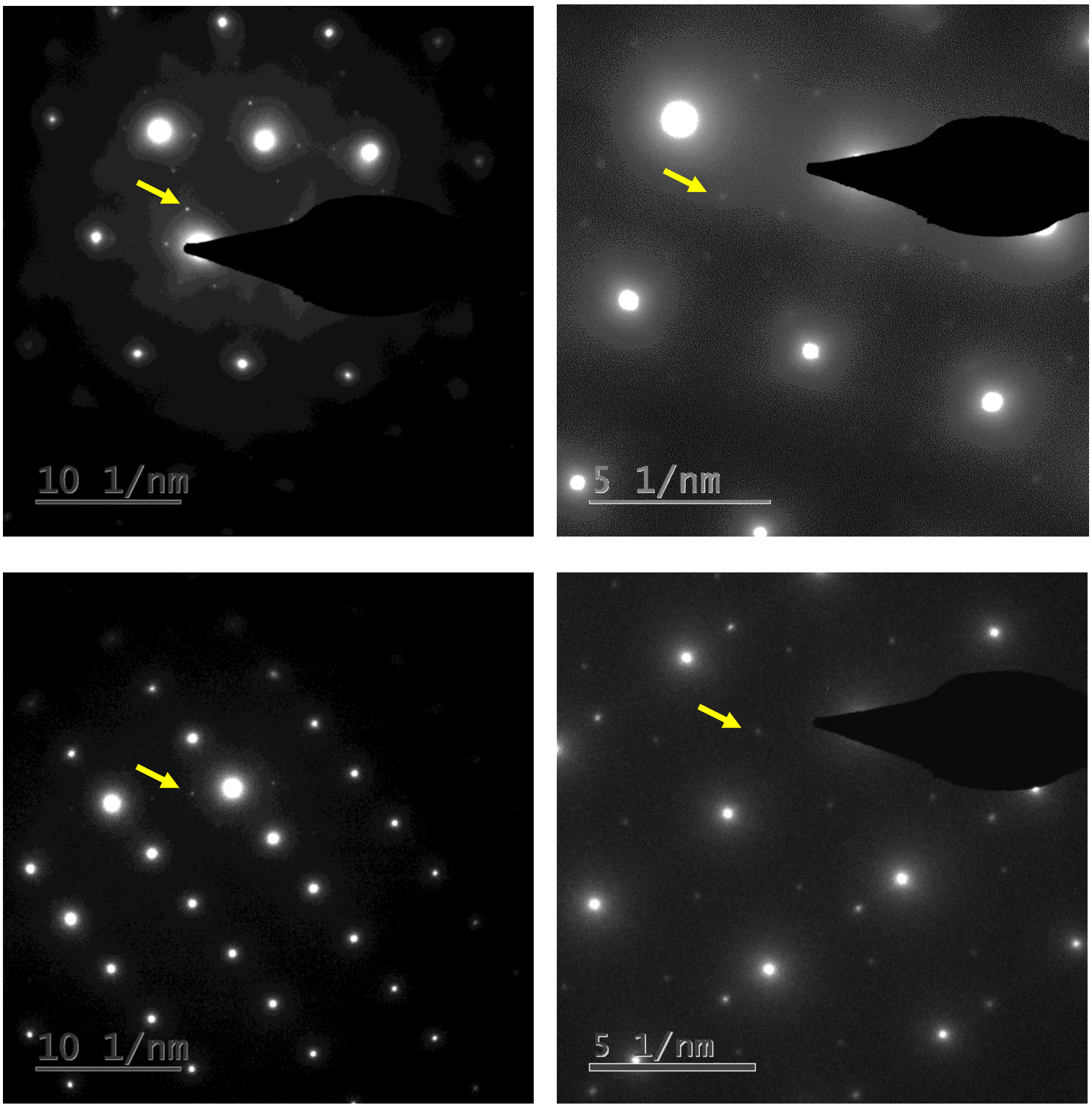

Figure 4.14 Secondary reflection in different zone axis (top left: [111], top right [001], bottom left [112], bottom right [011]). Superlattice reflection is arrowed out.

Table 4.2 TEM Diffraction pattern confirmation result in 2.0 samples.

Time (hrs)	**Unaged**	**3000**	**5000**
Temperature (°C)			
373	No	No	Untested
418	No	No	Untested
475	No	Yes	Yes

5 Conclusion

From the tests of XRD, micro-hardness, and TEM, following conclusions can be made: 1) Hardness result shows that decreasing Cr reduces the rate of ordering for off-stoichiometric samples at low temperature, 373℃. Stoichiometric samples have the fastest ordering rate. At high temperature, stoichiometric samples also have the fastest rate of ordering. The 2.4 composition sample, which is the farthest from stoichiometry, has the slowest rate of ordering. In 2.0 samples, TEM diffraction pattern result shows that there is no ordered phase before 3000 hours heat treatment at 373℃ and 418℃. Secondary phase starts to form after 1000 hours at 475℃. Both TEM and micro-hardness results have same conclusion. The result of 2.0 samples is consistent with the results from previous literature studies [4]. The plateau on ordering transformation, based on the explanation from Marucco [2], is the result of impinging between different ordered domains as their growth.

2) XRD result shows that ordering rate is similar for all compositions at low temperature. All compositions except sample 2.2 show lattice contraction after ageing for 3000 hours. At the medium temperature of 418℃, off-stoichiometric samples begin to show lattice contraction after 500 hours, but stoichiometric samples show lattice expansion. At high temperature,475℃, the 1.8 samples show faster contraction than other compositions. Stoichiometric samples still show lattice expansion instead of contraction. Many contraction measurements are much larger than 0.25% and this is expected to be attributed to residual stress from mechanical polishing and error of calculation on lattice parameter on identifying angle disturbed by oxide peak separation, which is of Ni_2O_3H structure.

3) It is difficult to conclude the relationship between stoichiometry and rate of ordering via XRD only because of the combination of three effects, which are

compressive effect from residual stress, expansion effect from releasing residual stress by heat treatment, and contraction effect from ordering transformation by ageing. Surface oxide makes precise angle identification even harder. This project has shown that hardness measurements describe the ordering rate better than XRD.

6 Future work

Considering the problems in current research result, several experimental techniques can be used to improve the conclusion and make research result applicable. First, the increase of micro-hardness is not large enough to clarify ordering behavior at low and medium temperatures. LRO characterization can be extended to samples with longer ageing time such as 10,000 hours at each temperature to obtain more obvious and stable result. TEM is able to calculate lattice parameter from diffraction pattern as well, but accuracy cannot be guaranteed to be stable because diffraction pattern comes from a small area, which makes local effects to be dominated on lattice parameter and the effect of ordering transformation is hard to be described.

Second, considering the tiny size of secondary phase, Atom Probe Tomography (APT) and neutron diffraction may have better effect on phase identification. APT is of higher resolution in atom scale imaging, which fits the size of ordered phase in Ni-Cr alloys. Neutron diffraction is of higher beam energy and lower sensitivity on surface condition, which can make result more robust to residual stress and surface oxide.

Third, considering ordering mechanism is diffusion based phase transformation, irradiation can be used to enhance phase transformation rate. Irradiation effect will also be explored due to service environment of Ni-Cr alloys.

Characterization on microstructure will also be extended to commercial alloys, such as Inconel 690 and 625, to make result more close to real situation.

Finally, the experimental data can be combined with the corresponding model called "Grizzly" in Multiphysics Object-Oriented Simulation Environment (MOOSE) framework to extend the model.

Bibliography

1. United States Nuclear Regulatory Commission, *The Pressurized Water Reactor (PWR)*. 2015.
2. Marucco, A. and B. Nath, *Effects of Ordering on the Properties of Ni-Cr Alloys.* Journal of Materials Science, 1988. **23**(6): p. 2107-2114.
3. Xiong, W., *Thermodynamic and kinetic investigation of the Fe-Cr-Ni system driven by engineering applications*, in *Department of Materials Science and Engineering*. 2012, KTH Royal Institute of Technology: School of Industrial Engineering and Management.
4. Marucco, A. *Effects of composition on the order-disorder transformation in ni-cr based alloys*. in *Key Engineering Materials*. 1991. Trans Tech Publ.
5. Young, G.A., J.D. Tucker, and D.R. Eno, *THE KINETICS OF LONG RANGE ORDERING IN NI-CR AND NI-CR-FE ALLOYS.* 2013.
6. Stojković, M., et al., *Structure and electronic properties of Mo 3 Pt, MoPt 2, and MoPt 3: First-principles calculations.* Physical Review B, 2008. **77**(19): p. 193111.
7. Nash, P., *Phase diagrams of binary nickel alloys.* ASM International(USA), 1991, 1991: p. 394.
8. Barnard, L., et al., *Atomistic modeling of the order–disorder phase transformation in the Ni 2 Cr model alloy.* Acta Materialia, 2014. **81**: p. 258-271.
9. Marucco, A., *Atomic ordering in the Ni Cr Fe system.* Materials Science and Engineering: A, 1994. **189**(1): p. 267-276.
10. Marucco, A., *Phase transformations during long-term ageing of Ni Fe Cr alloys in the temperature range 450–600° C.* Materials Science and Engineering: A, 1995. **194**(2): p. 225-233.
11. Avrami, M., *Kinetics of phase change. I General theory.* The Journal of Chemical Physics, 1939. **7**(12): p. 1103-1112.
12. Avrami, M., *Kinetics of phase change. II transformation ‐ time relations for random distribution of nuclei.* The Journal of Chemical Physics, 1940. **8**(2): p. 212-224.
13. Avrami, M., *Kinetics of phase change. III. Granulation, phase change, and microstructure.* J. chem. Phys, 1941. **9**(2): p. 177-184.
14. Johnson, W.A. and R.F. Mehl, *Reaction kinetics in processes of nucleation and growth.* Trans. Aime, 1939. **135**(8): p. 396-415.
15. Kolmogorov, A.N., *On the statistical theory of the crystallization of metals.* Bull. Acad. Sci. USSR, Math. Ser, 1937. **1**: p. 355-359.
16. Frely, E., et al., *Investigation of ordering kinetics in Ni-Cr-Fe alloys under electron irradiation.* Annales De Physique, 1997.
17. Delabrouille, F., et al. *Long Range Ordering of Alloy 690*. in *14th Intl. Conference on Environmental Degradation of Materials in Nuclear Power Systems, Virginia Beach, VA, USA*. 2009.
18. Young, G. and D. Eno, *Long range ordering in model Ni-Cr-X alloys*, in *Fontevraud 8 - Contribution of Materials Investigations and Operating Experience to LWRs' Safety,Performance and Reliability*. 2015: France, Avignon.

19. Frely, E., et al. *Short and Long-Range Ordering of (Ni 0.67 Cr 0.33) 1-x Fe x Alloys Under Electron Irradiation*. in *MRS Proceedings*. 1996. Cambridge Univ Press.
20. Marucco, A., *Atomic ordering and α′-Cr phase precipitation in long-term aged Ni3Cr and Ni2Cr alloys.* Journal of materials science, 1995. **30**(16): p. 4188-4194.
21. Verma, A., et al., *Delineating the roles of Cr and Mo during ordering transformations in stoichiometric Ni2(Cr1−x,Mox) alloys.* Acta Materialia, 2015. **96**: p. 366-377.
22. *Thermocouples*. Using Thermocouples to Measure Temperature; Available from: http://www.omega.com/prodinfo/thermocouples.html.
23. Kiker, E. *Choosing the right temperature sensor requires evaluation of the environment, temperature range, accuracy, and speed of response*. 2013; Available from: https://www.isa.org/standards-and-publications/isa-publications/intech-magazine/automation-basics/thermocouples-versus-rtds/.
24. B.D.Cullity, *Cohen's Method*, in *Elements of X-ray Diffraction* 1956, Addison-Wesley Publishing Company p. 338-342.
25. Iakoubovskii, K., et al., *Mean free path of inelastic electron scattering in elemental solids and oxides using transmission electron microscopy: Atomic number dependent oscillatory behavior.* Physical Review B, 2008. **77**(10): p. 104102.
26. Suryanarayana, C. and M.G. Norton, *X-ray diffraction: a practical approach*. 2013: Springer Science & Business Media.

7 Appendices

7.1 Appendix A. IMR Composition Confirmation Report

IMR TEST LABS
A Business Unit of CWST

131 Woodsedge Drive
Lansing, NY 14882

Toll Free 1.888.464.8422
Phone 1.607.533.7000
Fax 1.607.533.9210
Email imr@imrtest.com
Web www.imrtest.com

August 22, 2014

Julie Tucker
Oregon State University
204 Rodgers Hall
Corvallis, OR 97331

TEST REPORT

IMR Report Number 201410486

PO Number
P0096352

Date Received
August 15, 2014

Sample ID
Ni/Cr 1.6
Ni/Cr 1.8
Ni/Cr 2.0
Ni/Cr 2.2
Ni/Cr 2.4

SUMMARY

Five samples were received for chemical analysis.

The results are on the following page(s).

A2LA ACCREDITED
Testing Cert # 1140.01 & 1140.02

Accredited Nadcap
Materials Testing Laboratory

Reviewed by

Cheryl Downey
Report Review Specialist

Reviewed by

Andrew Ensign, Supervisor
Chemistry Department

CHEMISTRY

Element	Ni/Cr 1.6	Ni/Cr 1.8	Ni/Cr 2.0	Ni/Cr 2.2	Ni/Cr 2.4
C[1]	0.01	0.01	0.01	0.01	0.01
Cr	31.17	32.95	30.62	28.58	27.36
Fe	<0.01	<0.01	<0.01	<0.01	0.04
P	0.006	0.007	0.006	0.006	0.006
S[1]	0.002	0.002	0.002	0.002	0.001
Ni[2]	68.81	67.03	69.36	71.40	72.58

[1]Determined by combustion-infrared absorbance.
[2]Detrermined by difference.
Other elements tested (<0.01%): Al, As, Au, B, Be, Bi, Ca, Cd, Ce, Co, Cu, Hf, La, Li, Mg, Mn, Mo, Nb, Pb, Sb, Se, Si, Sn, Ta, Ti, V, W, & Zr.
Results in weight percent unless otherwise indicated.
Method(s): CAP-017N (ICP-AES) and ASTM E 1019-11 (Comb./IGF)

7.2 Appendix B. Calibration Data of Thermocouples

Thermocouple Calibration Data

11-16-2015

("+" stands for higher than setpoint, "-" stands for lower)

Thermocouple Model:	KTSS-116U-12	
Thermocouple Type (i.e. J,K or T)	K	
Tag Number (TC-Type-Year-#)	Setpoint value [℃]	Deviation [℃]
TC-K-15-001	300	-0.18
	400	-0.04
	500	-0.40
	600	-0.92
Calibration date	09-02-2015	
Notes		

Thermocouple Model:	KTSS-116U-12	
Thermocouple Type (i.e. J,K or T)	K	
Tag Number (TC-Type-Year-#)	Setpoint value [℃]	Deviation [℃]
TC- K-15-002	300	-1.32
	400	-1.56
	500	-1.28

	600	-1.88
Calibration date	09-02-2015	
Notes		

Thermocouple Model:	KTSS-116U-12	
Thermocouple Type (i.e. J,K or T)	K	
Tag Number (TC-Type-Year-#)	Setpoint value [℃]	Deviation [℃]
TC- K-15-003	300	-0.98
	400	-1.26
	500	-1.15
	600	-1.05
Calibration date	09-02-2015	

Thermocouple Model:	KTSS-116U-12	
Thermocouple Type (i.e. J,K or T)	K	
Tag Number (TC-Type-Year-#)	Setpoint value [℃]	Deviation [℃]
TC- K-15-004	300	+1.96
	400	+1.37
	500	+2.00
	600	+2.23
Calibration date	09-02-2015	
Notes		

Thermocouple Model:	KTSS-116U-12	
Thermocouple Type (i.e. J,K or T)	K	
Tag Number (TC-Type-Year-#)	Setpoint value [℃]	Deviation [℃]
TC- K-15-005	300	+1.85
	400	+1.70
	500	+1.94
	600	+1.76
Calibration date	09-02-2015	
Notes		

Thermocouple Model:	KTSS-116U-12	
Thermocouple Type (i.e. J,K or T)	K	
Tag Number (TC-Type-Year-#)	Setpoint value [℃]	Deviation [℃]
TC- K-15-006	300	+0.95
	400	+0.51
	500	+1.25
	600	+1.35
Calibration date	09-02-2015	
Notes		

Thermocouple Model:	TJ36-CAIN-18U-6

Thermocouple Type (i.e. J,K or T)	K	
Tag Number (TC-Type-Year-#)	Setpoint value [℃]	Deviation [℃]
TC- K-15-007	300	-0.85
	400	-1.00
	500	-0.30
	600	+0.15
Calibration date	09-02-2015	
Notes		

Thermocouple Model:	TJ36-CAIN-18U-6	
Thermocouple Type (i.e. J,K or T)	K	
Tag Number (TC-Type-Year-#)	Setpoint value [℃]	Deviation [℃]
TC- K-15-008	300	-0.25
	400	-1.40
	500	-0.50
	600	-0.28
Calibration date	09-02-2015	
Notes		

Thermocouple Model:	TJ36-CAIN-18U-6	
Thermocouple Type (i.e. J,K or T)	K	
Tag Number (TC-Type-Year-#)	Setpoint value [℃]	Deviation [℃]
TC- K-15-009	300	-0.60
	400	-1.03
	500	-0.93
	600	+0.19
Calibration date	09-02-2015	
Notes		

Thermocouple Model:	TJ36-CAIN-18U-6	
Thermocouple Type (i.e. J,K or T)	K	
Tag Number (TC-Type-Year-#)	Setpoint value [℃]	Deviation [℃]
TC- K-15-010	300	-0.50
	400	-1.48
	500	-0.40
	600	-0.34
Calibration date	09-02-2015	
Notes		

Thermocouple Model:	TJ36-CAIN-18U-6

Thermocouple Type (i.e. J,K or T)	K	
Tag Number (TC-Type-Year-#)	Setpoint value [℃]	Deviation [℃]
TC- K-15-011	300	-0.44
	400	-1.08
	500	-0.30
	600	+0.11
Calibration date	09-02-2015	
Notes		

Thermocouple Model:	TJ36-CAIN-18U-6	
Thermocouple Type (i.e. J,K or T)	K	
Tag Number (TC-Type-Year-#)	Setpoint value [℃]	Deviation [℃]
TC- K-15-012	300	-0.20
	400	-0.80
	500	-0.30
	600	+0.02
Calibration date	09-02-2015	
Notes		

Thermocouple Model:	TJ36-CAIN-18U-6	
Thermocouple Type (i.e. J,K or T)	K	
Tag Number (TC-Type-Year-#)	Setpoint value [℃]	Deviation [℃]
TC- K-15-013	300	-0.14
	400	+0.66
	500	+1.52
	600	+2.48
Calibration date	09-02-2015	
Notes		

Thermocouple Model:	TJ36-CAIN-18U-6	
Thermocouple Type (i.e. J,K or T)	K	
Tag Number (TC-Type-Year-#)	Setpoint value [℃]	Deviation [℃]
TC- K-15-014	300	-0.24
	400	-1.25
	500	-0.65
	600	-0.24
Calibration date	09-02-2015	
Notes		

Thermocouple Model:	TJ36-CAIN-18U-6

Thermocouple Type (i.e. J,K or T)	K	
Tag Number (TC-Type-Year-#)	Setpoint value [℃]	Deviation [℃]
TC- K-15-015	300	+0.16
	400	-1.13
	500	-0.40
	600	+0.40
Calibration date	09-02-2015	
Notes		

Thermocouple Model:	TJ36-CAIN-18U-6	
Thermocouple Type (i.e. J,K or T)	K	
Tag Number (TC-Type-Year-#)	Setpoint value [℃]	Deviation [℃]
TC- K-15-016	300	+0.67
	400	+0.80
	500	+1.34
	600	+1.98
Calibration date	09-02-2015	
Notes		

Thermocouple Model:	TJ36-CAIN-18U-6	
Thermocouple Type (i.e. J,K or T)	K	
Tag Number (TC-Type-Year-#)	Setpoint value [℃]	Deviation [℃]
TC- K-15-017	300	+0.63
	400	+0.74
	500	+1.34
	600	+1.80
Calibration date	09-02-2015	
Notes		

Thermocouple Model:	TJ36-CAIN-18U-6	
Thermocouple Type (i.e. J,K or T)	K	
Tag Number (TC-Type-Year-#)	Setpoint value [℃]	Deviation [℃]
TC- K-15-018	300	+0.64
	400	+0.49
	500	+1.58
	600	+2.58
Calibration date	09-02-2015	
Notes		

Thermocouple Model:	TJ36-CASS-316E-18

Thermocouple Type (i.e. J,K or T)	K	
Tag Number (TC-Type-Year-#)	Setpoint value [℃]	Deviation [℃]
TC- K-15-019	300	+0.78
	400	+1.17
	500	+1.62
	600	+1.13
Calibration date	09-02-2015	
Notes		

Thermocouple Model:	TJ36-CASS-316E-18	
Thermocouple Type (i.e. J,K or T)	K	
Tag Number (TC-Type-Year-#)	Setpoint value [℃]	Deviation [℃]
TC- K-15-020	300	-0.03
	400	+0.01
	500	+0.89
	600	+0.95
Calibration date	09-02-2015	
Notes		

Thermocouple Model:	TJ36-CASS-316E-18	
Thermocouple Type (i.e. J,K or T)	K	
Tag Number (TC-Type-Year-#)	Setpoint value [℃]	Deviation [℃]
TC- K-15-021	300	-0.08
	400	-0.20
	500	+0.52
	600	+0.51
Calibration date	09-02-2015	
Notes		

Thermocouple Model:	TJ36-CASS-316E-18	
Thermocouple Type (i.e. J,K or T)	K	
Tag Number (TC-Type-Year-#)	Setpoint value [℃]	Deviation [℃]
TC- K-15-022	300	+3.96
	400	+4.76
	500	+5.65
	600	+5.26
Calibration date	09-02-2015	
Notes	Large Temperature Deviation	

Thermocouple Model:	TJ36-CASS-316E-18

Thermocouple Type (i.e. J,K or T)	K	
Tag Number (TC-Type-Year-#)	Setpoint value [℃]	Deviation [℃]
TC- K-15-023	300	+3.70
	400	+4.07
	500	+5.01
	600	+5.46
Calibration date	09-02-2015	
Notes	Large Temperature Deviation	

Thermocouple Model:	K-316SS18-U-T3	
Thermocouple Type (i.e. J,K or T)	K	
Tag Number (TC-Type-Year-#)	Setpoint value [℃]	Deviation [℃]
TC- K-15-024	300	+0.26
	400	+0.24
	500	+0.74
	600	+0.64
Calibration date	10-06-2015	
Notes		

Thermocouple Model:	K-316SS18-U-T3	
Thermocouple Type (i.e. J,K or T)	K	
Tag Number (TC-Type-Year-#)	Setpoint value [℃]	Deviation [℃]
TC- K-15-025	300	-0.08
	400	-0.20
	500	-0.14
	600	+0.75
Calibration date	10-06-2015	
Notes		

Thermocouple Model:	K-316SS18-U-T3	
Thermocouple Type (i.e. J,K or T)	K	
Tag Number (TC-Type-Year-#)	Setpoint value [℃]	Deviation [℃]
TC- K-15-026	300	+0.01
	400	-0.29
	500	+0.34
	600	+0.71
Calibration date	10-06-2015	
Notes		

Thermocouple Model:	K-316SS18-U-T3

Thermocouple Type (i.e. J,K or T)	K	
Tag Number (TC-Type-Year-#)	Setpoint value [℃]	Deviation [℃]
TC- K-15-027	300	-0.04
	400	-0.25
	500	-0.10
	600	+0.57
Calibration date	10-06-2015	
Notes		

Thermocouple Model:	K-316SS18-U-T3	
Thermocouple Type (i.e. J,K or T)	K	
Tag Number (TC-Type-Year-#)	Setpoint value [℃]	Deviation [℃]
TC- K-15-028	300	-0.01
	400	-0.23
	500	+0.39
	600	+0.58
Calibration date	10-06-2015	
Notes		

Thermocouple Model:	K-316SS18-U-T3	
Thermocouple Type (i.e. J,K or T)	K	
Tag Number (TC-Type-Year-#)	Setpoint value [℃]	Deviation [℃]
TC- K-15-029	300	-0.70
	400	-0.50
	500	-0.10
	600	+1.00
Calibration date	10-07-2015	
Notes		

Thermocouple Model:	K-316SS18-U-T3	
Thermocouple Type (i.e. J,K or T)	K	
Tag Number (TC-Type-Year-#)	Setpoint value [℃]	Deviation [℃]
TC- K-15-030	300	-0.30
	400	-0.70
	500	+0.20
	600	+0.20
Calibration date	10-07-2015	
Notes		

Thermocouple Model:	C1035-

Thermocouple Type (i.e. J,K or T)	K	
Tag Number (TC-Type-Year-#)	Setpoint value [℃]	Deviation [℃]
TC- K-15-031	300	+0.85
	400	+0.945
	500	+0.744
	600	+1.25
Calibration date	11-04-2015	
Notes		

Thermocouple Model:	C1035-	
Thermocouple Type (i.e. J,K or T)	K	
Tag Number (TC-Type-Year-#)	Setpoint value [℃]	Deviation [℃]
TC- K-15-032	300	+3.95
	400	+4.245
	500	+4.544
	600	+4.75
Calibration date	11-04-2015	
Notes		

Thermocouple Model:	C1035-	
Thermocouple Type (i.e. J,K or T)	K	
Tag Number (TC-Type-Year-#)	Setpoint value [℃]	Deviation [℃]
TC- K-15-033	300	+2.05
	400	+2.345
	500	+2.844
	600	+3.05
Calibration date	11-04-2015	
Notes		

Thermocouple Model:	C1035-	
Thermocouple Type (i.e. J,K or T)	K	
Tag Number (TC-Type-Year-#)	Setpoint value [℃]	Deviation [℃]
TC- K-15-034	300	+4.55
	400	+4.845
	500	+5.844
	600	+5.35
Calibration date	11-04-2015	
Notes		

Thermocouple Model:	C1035-

Thermocouple Type (i.e. J,K or T)	K	
Tag Number (TC-Type-Year-#)	Setpoint value [℃]	Deviation [℃]
TC- K-15-035	300	+3.25
	400	+2.845
	500	+3.444
	600	+3.35
Calibration date	11-04-2015	
Notes		

7.3 Appendix C. Calibration procedures

<table>
<tr><td colspan="2">CALB Report Number: OSU-NMM-CALB-001-

Thermocouple</td><td>Revision: 0</td><td>Addendum:0</td></tr>
<tr><td colspan="4">Quality Document:

☐ Yes
☐ No</td></tr>
<tr><td colspan="4">CALB Report Title:

OSU NMM – Thermocouple Calibration</td></tr>
<tr><td colspan="4">Purpose:

Identify all steps and documentation necessary to perform a thermocouple calibration.</td></tr>
<tr><td colspan="4">Affected Document(s): OSU-NMM-SOP-001-Isothermal Aging</td></tr>
<tr><td>Prepared By:</td><td>Signature</td><td colspan="2">Date</td></tr>
<tr><td>Reviewed By:</td><td>Signature</td><td colspan="2">Date</td></tr>
</table>

Approved By:	**Signature**	**Date**

OSU NMM – Thermocouple Calibration

OSU-NMM-CALB-001-Thermocouple

Prepared by:

Department of Mechanical, Industrial Manufacturing Engineering

Oregon State University

204 Rogers Hall

Corvallis, OR 97331-6001

TABLE OF CONTENTS

Section Page

LIST OF TABLES

LIST OF ACRONYMS

OSU	Oregon State University
PPE	Personal Protection Equipment
NMM	Nuclear Material and Metallurgy Group

1 PURPOSE

This procedure identifies all steps and documentation necessary to perform a thermocouple calibration. As stated in OSU-NMM-SOP-001-Isothermal Aging, thermocouples require repeated calibration if sufficient temperature deviation occurs or thermocouples have served for one year, whichever comes first.

2 SCOPE

This procedure was developed to calibrate any standard or high precision K-Type thermocouple.

3 INITIAL CONDITIONS

Instrumentation is up for re-calibration, is deemed out of calibration or was received by a manufacturer with insufficient information to support program quality requirements for calibration.

4 PERSONNEL

This procedure requires at least one qualified and trained Instrumentation and Calibration Technician to directly perform or provide oversight of all steps outlined herein.

Table 4.1: Personnel Conducting Procedure

Printed Name	Signature	Initials	Date
Fei Teng			

5 PERSONAL PROTECTION EQUIPMENT

Personal Protection Equipment (PPE) consists of the following for this procedure:

- Insulated gloves

6 TOOLS AND MATERIALS

- Dry well tester, 9144-A Field Metrology Well or equivalent (tester)
- Thermocouple
- 1502A Thermometer Readout
- 5609 Platinum Resistance Thermometer

7 PROCEDURE

1. Verify thermocouple dry well tester is within its required calibration periodicity.
   Record the following information from the calibration label located on the drywell:
    - 1.a. Model Number: FLUKE 9144 & 5609 Pt Resistance Thermometer
    - 1.b. Serial Number: B5A005 (for 9144) & 03830 (for Thermometer)
    - 1.c. Calibration Date: 10/01/2015
    - 1.d. Date Calibration Due: 01/14/2018(for metal sheath) & 05/05/2016(for Digital Thermometer)
2. Setup Calibration hardware configuration
    - 2.a. Prepare the drywell
        - 2.a.xxii. Use arrows to set a value of 300.00 ºC
        - 2.a.xxiii. Press ENTER
        - 2.a.xxiv. Use arrows to highlight “PRESET 2:” value.
        - 2.a.xxv. Press ENTER
        - 2.a.xxvi. Use arrows to set a value of 400.00 ºC
        - 2.a.xxvii. Press ENTER
        - 2.a.xxviii. Use arrows to highlight “PRESET 3:” value.
        - 2.a.xxix. Press ENTER
        - 2.a.xxx. Use arrows to set a value of 500.00 ºC
        - 2.a.xxxi. Press ENTER
        - 2.a.xxxii. Use arrows to highlight “PRESET 4:” value.

2.a.xxxiii. Press ENTER

2.a.xxxiv. Use arrows to set a value of 600.00 ºC

2.a.xxxv. Press EXIT

2.a.xxxvi. If not already, insert the 9144-A insert into the drywell receiver hole.

2.b. Prepare the thermocouple

2.b.i. Connect the thermocouple leads to the computer with LabView program, observing correct polarity.

2.b.ii. Record the ambient temperature as measured by the thermocouple on the tester to the nearest tenth of a degree on Table 2.1.

2.b.iii. Insert the thermocouple into the computer.

3. Set the tester controller to 300.0 °C. Allow sufficient time for the tester, insert, and thermocouple to reach steady-state at the setpoint.
4. Record the temperature as read by the thermocouple on the computer to the nearest tenth of a degree in Table 7.1.
5. Set the tester controller to 400.0 °C. Allow sufficient time for the tester, insert, and thermocouple to reach steady-state at the setpoint.
6. Record the temperature as read by the thermocouple on the computer to the nearest tenth of a degree in Table 7.1.
7. Set the tester controller to 500.0 °C. Allow sufficient time for the tester, insert, and thermocouple to reach steady-state at the setpoint.
8. Record the temperature as read by the thermocouple on the computer to the nearest tenth of a degree in Table 7.1.
9. Set the tester controller to 600.0 °C. Allow sufficient time for the tester, insert, and thermocouple to reach steady-state at the setpoint.
10. Record the temperature as read by the thermocouple on the computer to the nearest tenth of a degree in Table 7.1.
11. Verify each recorded value is within the accuracy limits listed in logbook. If the thermocouple reading is not within these limits, make a note in “Notes” section and place it in an out-of-service state and replace it with a new thermocouple of the same model number or equivalent and repeat this procedure.
12. Remove thermocouple from computer.
13. Reduce the tester controller setpoint to less than 30 °C and allow tester to reach

steady-state at the setpoint.

14. Secure the thermocouple in its respective location within the Oregon State University (OSU) Nuclear Material and Metallurgy lab (NMM) and attach its lead ends to the appropriate terminal block location in the OSU NMM lab box.
15. Provide detail of any deviations to this procedure in detail using logbook.
16. Transpose all relevant calibration data from Table 7.1 into a new revision of thermocouple's Instrumentation Calibration Record and archive the old Instrumentation Calibration Record in the appropriate location.
17. Create and affix a calibration label to the thermocouple.
28. Return the thermocouple to service as follows:
    20.a. Re-install on the facility.
    20.b. Align the thermocouple with the data acquisition system (DAS) or programmable logic controller (PLC) and update any other DAS or PLC affected parameters (set points, alarms, etc.).

Table 7.1: Thermocouple calibration data

<table>
<tr><td>Thermocouple Model:</td><td colspan="2"></td></tr>
<tr><td>Thermocouple Type (i.e. J,K or T)</td><td colspan="2"></td></tr>
<tr><td>Tag Number (TC-Type-Year-#)</td><td>Setpoint value [℃]</td><td>Deviation [℃]</td></tr>
<tr><td rowspan="4">TC-K-______</td><td>300</td><td></td></tr>
<tr><td>400</td><td></td></tr>
<tr><td>500</td><td></td></tr>
<tr><td>600</td><td></td></tr>
<tr><td>Calibration date</td><td colspan="2"></td></tr>
<tr><td>Notes</td><td colspan="2"></td></tr>
</table>

CALIBRATION RECORD DEFINITIONS

The following is a list of definitions for the terms contained in attachment A, the thermocouple calibration record, of this document:

Tag #	Instrument tag number (e.g. TC-K-15-001)
Model #	Instrument model number determined by manufacturer.
Serial #	The number given by the manufacturer to uniquely identify one instrument of a particular model type.
Procedure #	The particular document which contains the calibration procedure for the instrument in question.
Field Range	The upper and lower limit of the instrument after being installed in the facility and having performed any necessary compensation. Values are in the instrument's respective engineering units.
Cal. Range	The range necessary to calibrate the instrument within. May be larger than the field range. Values are in the instrument's respective engineering units.
ENGR Units	Engineering units read out in DAS or PLC based on instrument signal type.
Procedure Title	The title of document containing the calibration procedure.
Date	The present date that the calibration is being performed on.
Date Due	Last date calibration may be performed without voiding calibration certificate.

Drawing	Drawing referencing location of instrument.
As Found Data	Measurements of setpoint data taken by the instrument prior to calibration.
% of Span	Gives the percentage of the applied process variable out of the maximum allowed value.
Applied	The known process variable applied to the sensor.
Required	The range within which the analog output of the instrument must lie in order for the instrument to be considered within calibration.
% Span Error	The percent span error gives the error in the analog output as a percentage of the total range. The formula for this error is:

$$\%Span\ Error = \left(\frac{(ourput\ reading) - (lower\ output\ range)}{(upper\ output\ range) - (lower\ output\ range)}\right) * 100 - (Applied\ Span\ \%)$$

Test Equipment	The equipment used in the calibration of the instrument.
Vendor	The company which supplied the test equipment used for calibration.
Accuracy	The accuracy of the test equipment, determined by calibrating the test equipment.
Cal. Date	The date of the most recent calibration of the test equipment used for recalibration of the instrumentation.
Cal. Due Date	The date when the test equipment must be recalibrated to ensure accuracy, generally 18 months after the most recent calibration date.

ATTACHMENT A: Raw data files

ATTACHMENT B: Notes from calibration procedure

Name: ____________________ _______________________ _______________

(Last) (First) (MI)

Notes:

ATTACHMENT C: Thermocouple calibration tables